NASA CONTRACTOR REPORT

NASA CR-2207

NASA CR-2207

CYCLIC DEBONDING OF ADHESIVE JOINTS: SUMMARY REPORT

by D. J. Hoffman and R. R. June

Prepared by
BOEING COMMERCIAL AIRPLANE COMPANY
Seattle, Wash. 98124
for Langley Research Center

NATIONAL AERONAUTICS AND SPACE ADMINISTRATION • WASHINGTON, D. C. • JUNE 1973

1. Report No.	2. Government Accession No.	3. Recipient's Catalog No.
NASA CR-2207		

4. Title and Subtitle	5. Report Date
CYCLIC DEBONDING OF ADHESIVE JOINTS: SUMMARY REPORT	June 1973
	6. Performing Organization Code
7. Author(s)	8. Performing Organization Report No.
D. J. Hoffman and R. R. June	D6-60136-5
9. Performing Organization Name and Address	10. Work Unit No.
Boeing Commercial Airplane Company P.O. Box 3707 Seattle, Washington 98124	11. Contract or Grant No. NAS 1-8858
12. Sponsoring Agency Name and Address	13. Type of Report and Period Covered
National Aeronautics and Space Administration Washington, D.C. 20546	Contractor Report
	14. Sponsoring Agency Code

15. Supplementary Notes

16. Abstract

Bonded lap joints were manufactured and tested under static and fatigue loading. Specimens were designed to fail in the bondline, and all fatigue tests included monitoring the crack growth to failure. Detailed crack length readings for 106 fatigue specimens are contained in NASA CR-112219–*Cyclic Debonding of Adhesive Joints: Data Report.*

Test specimens included aluminum details joined by two different adhesives. Specimens also included titanium and boron-epoxy details joined by an epoxy laminating resin. Additional program variables included bondline thickness, adherend and spice plate thickness, specimen width, and specimen fabrication procedure.

Adhesive aging, a previously unobserved effect, was found to be generally detrimental to the lives of most of the specimens bonded with one adhesive system. Adhesive material was found to have a major influence on debond rate. Co-cured titanium/boron-epoxy specimens were found to resist debonding better than specimens fabricated with a sequential cure. Splice plate thickness and test section width were found to have little effect on debond rate. The data also suggested the existence of an optimum bondline thickness.

17. Key Words (Suggested by Author(s))	18. Distribution Statement
Debonding Adhesive Fatigue Bonded joints Filamentary composites Boron-epoxy	Unclassified–Unlimited

19. Security Classif. (of this report)	20. Security Classif. (of this page)	21. No. of Pages	22. Price*
Unclassified	Unclassified	73	$3.00

*For sale by the National Technical Information Service, Springfield, Virginia 22151

FOREWORD

This report was prepared by the Boeing Commercial Airplane Company under NASA contract NAS1-8858 and covers work performed during the period June 1971 through October 1972, on Phase III of a three-phase contract.

The authors wish to acknowledge the contributions of the following Boeing structural test personnel:

W. C. Larson
T. E. Kane

CONTENTS

	Page
SUMMARY	1
INTRODUCTION	3
SYMBOLS	5
OBJECTIVE	7
BACKGROUND AND APPROACH	7
EXPERIMENTAL TEST PROGRAM	11
TEST SPECIMEN DESIGN AND FABRICATION	15
TEST PROCEDURE	21
Static Tests	21
Fatigue Tests	21
TEST RESULTS AND DISCUSSION OF RESULTS	27
Static Tests	27
Fatigue Tests	28
CONCLUSIONS	57
RECOMMENDATIONS	59
APPENDIX A—Conversion of SI Units to U.S. Customary Units	61
APPENDIX B—Test Specimen Materials	63
APPENDIX C—Test Specimen Fabrication Procedures	67
REFERENCES	69

CYCLIC DEBONDING OF ADHESIVE JOINTS: SUMMARY REPORT

By D. J. Hoffman and R. R. June
Boeing Commercial Airplane Company

SUMMARY

This report summarizes an experimental investigation into the failure of adhesive bondlines and advanced-composite matrix materials subjected to fatigue loading. The failure of these materials due to this type of loading is referred to as cyclic debonding of adhesive joints. Detailed crack growth data for the 106 fatigue specimens involved are presented in NASA CR-112219, *Cyclic Debonding of Adhesive Joints: Data Report* (ref. 1).

This work was accomplished as an extension to Phase III of a three-phase program performed to establish the feasibility of reinforcing metal aircraft structures with advanced filamentary composites (refs. 2-4). Data obtained in Phase II of the program (ref. 3) demonstrated a need for additional understanding of the behavior of these materials subjected to cyclic loading.

All materials involved in this program were the same as those used previously in the Phase II work. The majority of the cyclic debonding specimens consisted of aluminum components joined by a modified epoxy adhesive. A lesser number of specimens consisted of titanium and boron-epoxy components joined by the epoxy laminating resin. The material systems that were investigated are described in detail in appendix B.

A single-lap splice specimen was selected for study. Program variables included:

- Bondline thickness (configurations 1, 2, and 3)
- Adherend and splice plate thickness (configurations 4 and 5)
- Specimen width (configuration 6)
- Adhesive material (configurations 1 and 7)
- Adherend and splice material (configurations 8 and 9)

This investigation demonstrated the feasibility of monitoring fatigue crack growth in adhesive bondlines. The use of a fluorescent dye penetrant provided a simple but accurate means of recording the crack length. This method gave the added advantage of leaving a permanent record of debond lengths on the failure surface.

A majority of the specimens using one of the adhesive systems were affected by adhesive aging. Generally this aging was found to be detrimental to specimen life. Additional investigation should be performed in this area.

Adhesive or matrix material was found to influence debond rate more than any other program variable.

The co-cure method of fabricating titanium/boron-epoxy specimens was found to provide considerably more resistance to debonding than the sequential-cure method.

Bondline thickness was also found to influence debond rate. The data suggested an optimum bondline thickness.

Splice plate thickness to adherend thickness ratio also influenced debond rate. As this ratio increased, the debond rate also increased.

Specimen width was found to have little influence on the initial crack growth rate.

INTRODUCTION

Previous investigations have demonstrated that the application of advanced filamentary composites to aircraft structure can result in significant weight savings. The cyclic debonding work described in this report was performed under an extension to Phase III (ref. 4) of a three-phase contract designed to demonstrate the advantages of selective use of composites as reinforcement to metal structure. Work performed in the three-phase contract ranged from material selection and development of bonding techniques to fabrication and test of three full-size components involving the complex design features of typical aircraft structure. The results amply demonstrated both the feasibility and the advantages associated with this type of construction.

As with any new material system and structural concept, some areas were discovered that warranted additional investigation. One such area involved the fatigue and crack growth tests performed in Phase II (ref. 3). The results of these tests showed that the fatigue-critical component in this type of structure was the matrix material or the adhesive used to join the various components in load transfer and joint regions.

Previous use of bonding in aircraft has been confined to relatively lightly loaded secondary structure. In these applications the adhesive has normally not been the fatigue-critical component. The potential use of bonded primary aircraft structure and the application of advanced filamentary composites changes this picture. The adhesive or matrix material now becomes the fatigue-critical component. In order to improve the fatigue performance of these structures it will be necessary to understand the phenomenon of debonding of adhesive joints subjected to cyclic loads.

SYMBOLS

Physical quantities defined in this paper are given in both the international system of units (SI, ref. 5) and the U.S. customary units. Conversion factors pertinent to the present investigation are presented in appendix A.

a crack length, millimeters (inches)

b width of test section, millimeters (inches)

F allowable stress, newtons per square meter (pounds per square inch)

K_t stress concentration factor, nondimensional

ℓ lap length, millimeters (inches)

N number of load cycles, nondimensional

R ratio of maximum applied stress to minimum applied stress, nondimensional

T temperature, degrees Kelvin (Fahrenheit)

t thickness, millimeters (inches)

ϵ axial strain, %, nondimensional

σ maximum applied fatigue stress, newtons per square meter (pounds per square inch)

Subscripts

a adherend

ad adhesive or matrix

sp splice plate

t tension

y yield

OBJECTIVE

The objective of this investigation was to provide debonding data on adhesive and matrix materials subjected to fatigue loading in ambient environment. The program was centered around a series of tests designed to determine the effects of various parameters on debond rate.

BACKGROUND AND APPROACH

The results of fatigue tests performed in Phase II showed that the fatigue-critical component for the specimens tested was the matrix material or the adhesive used to join the composite to the metal in the load transfer region. Among the specific conclusions reached were the following:

- The fatigue life of the reinforced specimens was determined by the load transfer region design and the matrix performance.

- Further improvements in fatigue performance may be possible by changing the load transfer region design to lower the adhesive stresses.

Figure 1 shows an aluminum/boron-epoxy step joint specimen that had been fatigue tested as part of the Phase II work. The debonding of the fibers from the steps is clearly visible.

The results of crack propagation and residual strength tests performed in Phase II also showed the influence of adhesive and matrix performance. Tests were run on center-notched flat panels utilizing one of the following structural concepts:

- Honeycomb with distributed reinforcement
- Honeycomb with concentrated reinforcement
- Hat stringers with simple skin
- Hat stringers with honeycomb skins

Of the four basic structural concepts tested, three concepts experienced debonding. In at least one instance it was observed that crack growth in the panel was accompanied by debonding. Figure 2 shows a sketch of the test section of a panel tested during the Phase II work where the extent of the primary fatigue crack is clearly related to the delamination boundary line, i.e., debonding. These tests indicate the importance of the performance of matrix and adhesive components in structures selectively reinforced with advanced composite. An understanding of the stresses present in these components and how various design parameters influence their magnitude is equally important.

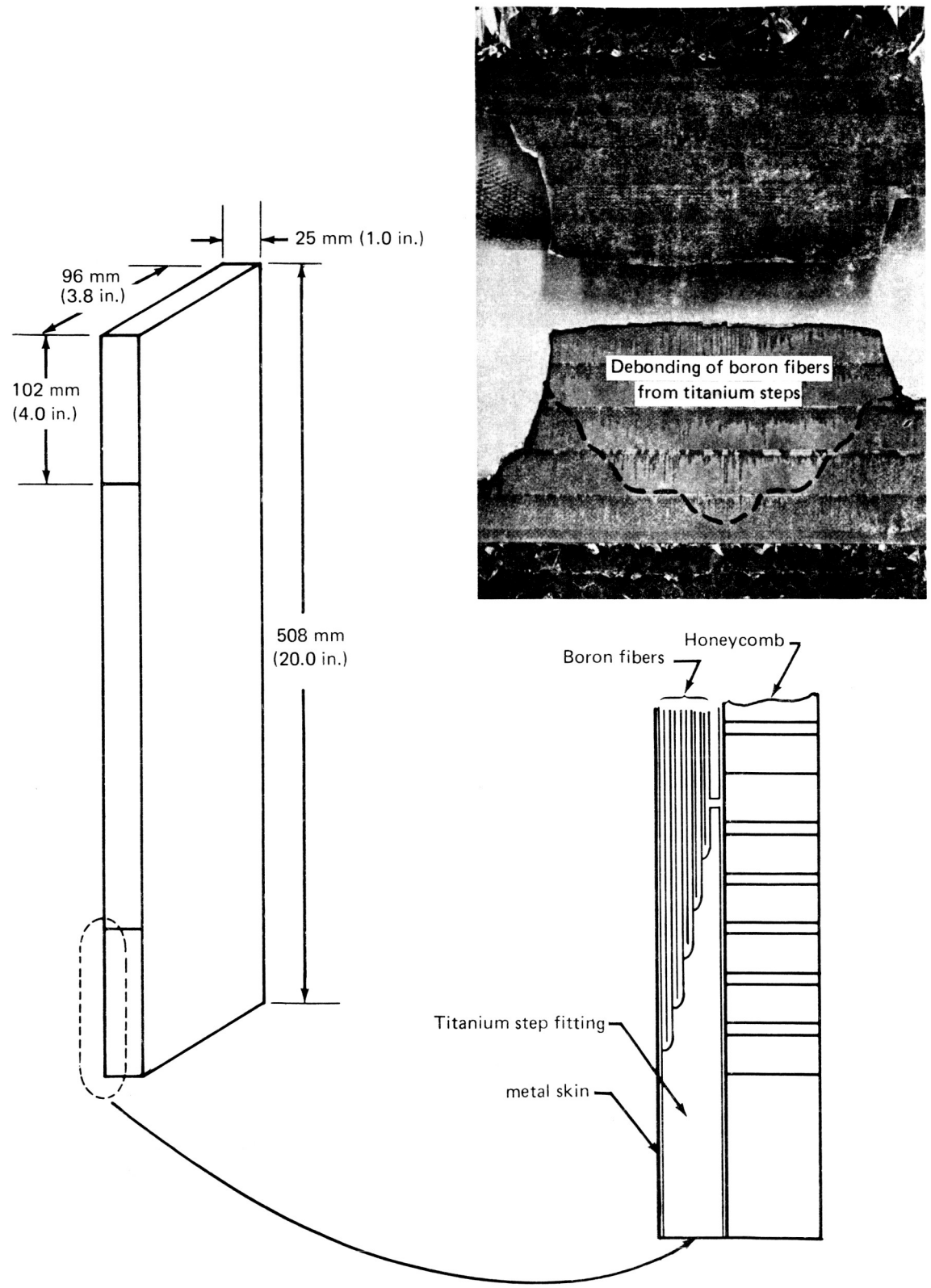

FIGURE 1.–PHASE II DEBONDED FATIGUE SPECIMEN

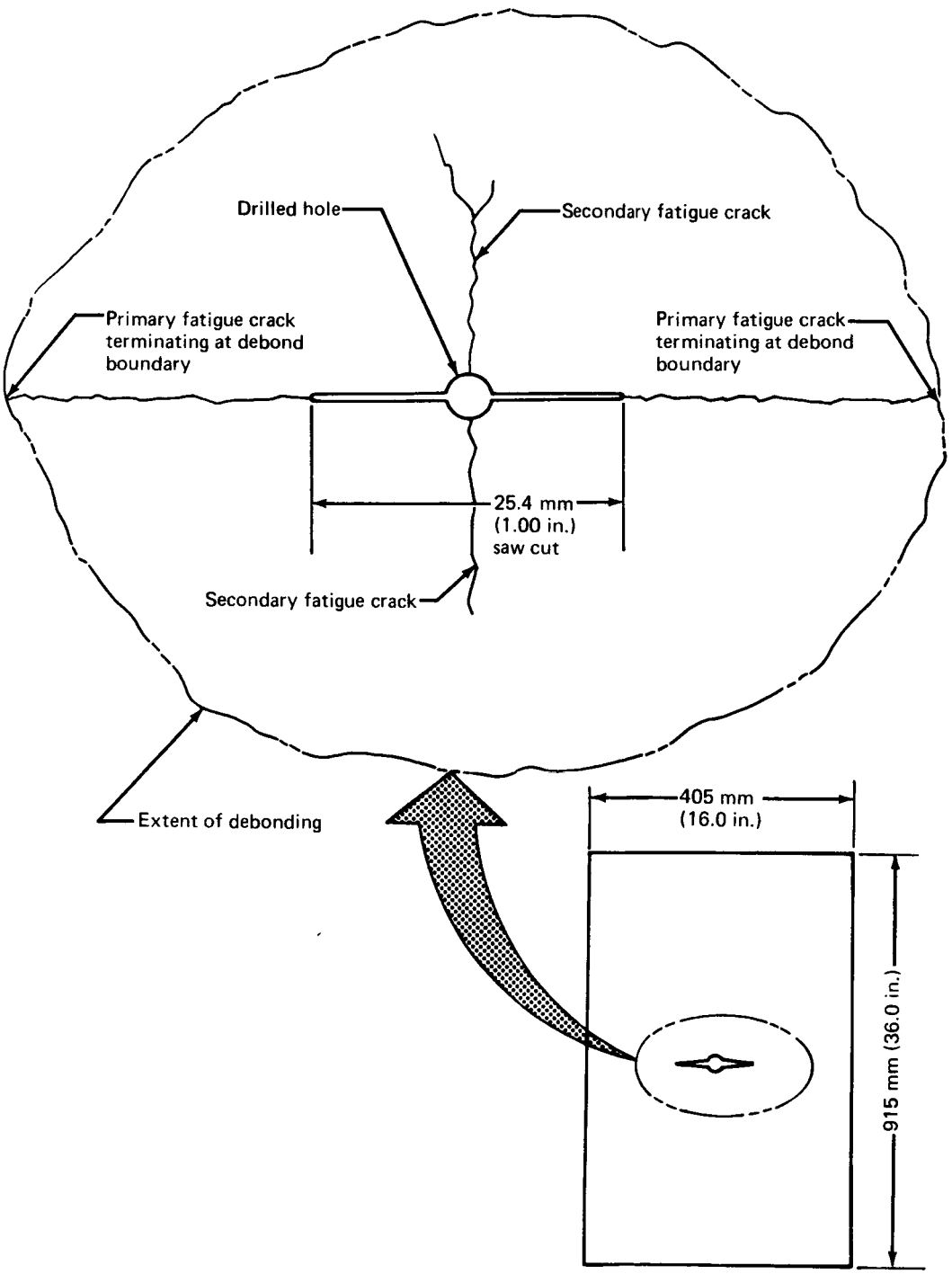

FIGURE 2.–SIMULTANEOUS OCCURRENCE OF DEBONDING AND SKIN CRACK GROWTH

EXPERIMENTAL TEST PROGRAM

The experimental test program plan is shown in table 1. Two static tests were required for each configuration plus three fatigue tests at each of three or four load levels. The static tests were included to verify specimen quality and to establish ultimate failure load and mode. In all fatigue tests, crack growth was monitored to failure. Fatigue test loads were chosen to provide specimen lives in the range of 10^4 to 10^5 cycles.

The specimen proposed for use in the debonding program is shown in figure 3. It consisted of a simple lap splice requiring complete load transfer from the adherend through the bondline to the splice plate. The majority of the specimens had aluminum adherends because surface preparation and general joint fabrication technology are more advanced for aluminum bonding than for titanium and advanced-composite bonding. The program required high-quality, uniform-thickness bondlines; it was believed that these could best be obtained with aluminum specimens. Use of the relatively inexpensive aluminum specimens also helped to reduce specimen costs. A lesser number of titanium/boron-epoxy specimens were also tested. These were included in order to examine the effect of the adherend material on debond rate and to provide a material combination identical to one of those tested in the Phase II work.

Not all of the factors that could influence debond rate were investigated; in fact, some parameters were omitted that could have a major effect on debond rate. Instead, the program concentrated on controllable geometric parameters and some material variation. Variables included:

- Bondline thickness (configurations 1, 2, and 3)
- Adherend and splice plate thickness (configurations 4 and 5)
- Specimen width (configuration 6)
- Adhesive material (configurations 1 and 7)
- Adherend and splice material (configurations 8 and 9)

Configuration 8 was co-cured: the matrix of the boron-epoxy prepreg tape was the adhesive. Configuration 9 used an additional layer of laminating resin to bond precured composite to the metal.

TABLE 1.—EXPERIMENTAL TEST PROGRAM PLAN

Configuration	Adhesive material	Nominal adhesive thickness, t_{ad}, mm (in.)	Adherend material	Nominal adherend thickness, t_a, mm (in.)	Splice plate material	Nominal splice plate thickness, t_{sp}, mm (in.)	Test section width, b. mm (in.)	Number of static specimens required	Number of fatigue specimens required
1	AF-126	0.127 (0.005)	7075-T6	3.175 (0.125)	7075-T6	6.350 (0.250)	38.1 (1.50)	2	3 specimens at each of 4 load levels
2	AF-126	0.254 (0.010)	7075-T6	3.175 (0.125)	7075-T6	6.350 (0.250)	38.1 (1.50)	2	3 specimens at each of 4 load levels
3	AF-126	0.508 (0.020)	7075-T6	3.175 (0.125)	7075-T6	6.350 (0.250)	38.1 (1.50)	2	3 specimens at each of 4 load levels
4	AF-126	0.127 (0.005)	7075-T6	3.175 (0.125)	7075-T6	4.826 (0.190)	38.1 (1.50)	2	3 specimens at each of 3 load levels
5	AF-126	0.127 (0.005)	7075-T6	4.064 (0.160)	7075-T6	4.826 (0.190)	38.1 (1.50)	2	3 specimens at each of 3 load levels
6	AF-126	0.127 (0.005)	7075-T6	3.175 (0.125)	7075-T6	6.350 (0.250)	76.2 (3.00)	2	3 specimens at each of 4 load levels
7	BP907	0.076 (0.003)	7075-T6	3.175 (0.125)	7075-T6	6.350 (0.250)	38.1 (1.50)	2	3 specimens at each of 4 load levels
8	BP907	[a]0.000 (0.000)	Ti-6Al-4V	1.600 (0.063)	Boron-epoxy	[b]1.803 (0.071)	38.1 (1.50)	2	3 specimens at each of 4 load levels
9	BP907	0.076 (0.003)	Ti-6Al-4V	1.600 (0.063)	Boron-epoxy	[b]1.803 (0.071)	38.1 (1.50)	2	3 specimens at each of 4 load levels

[a]Co-cure situation where no adhesive is added as a bonding agent. Adhesion is achieved by matrix material in pre-preg tape.

[b]Based on 13 plies of uniaxial boron-epoxy with an estimated average thickness per ply of 0.1397 mm (0.0055 in.)

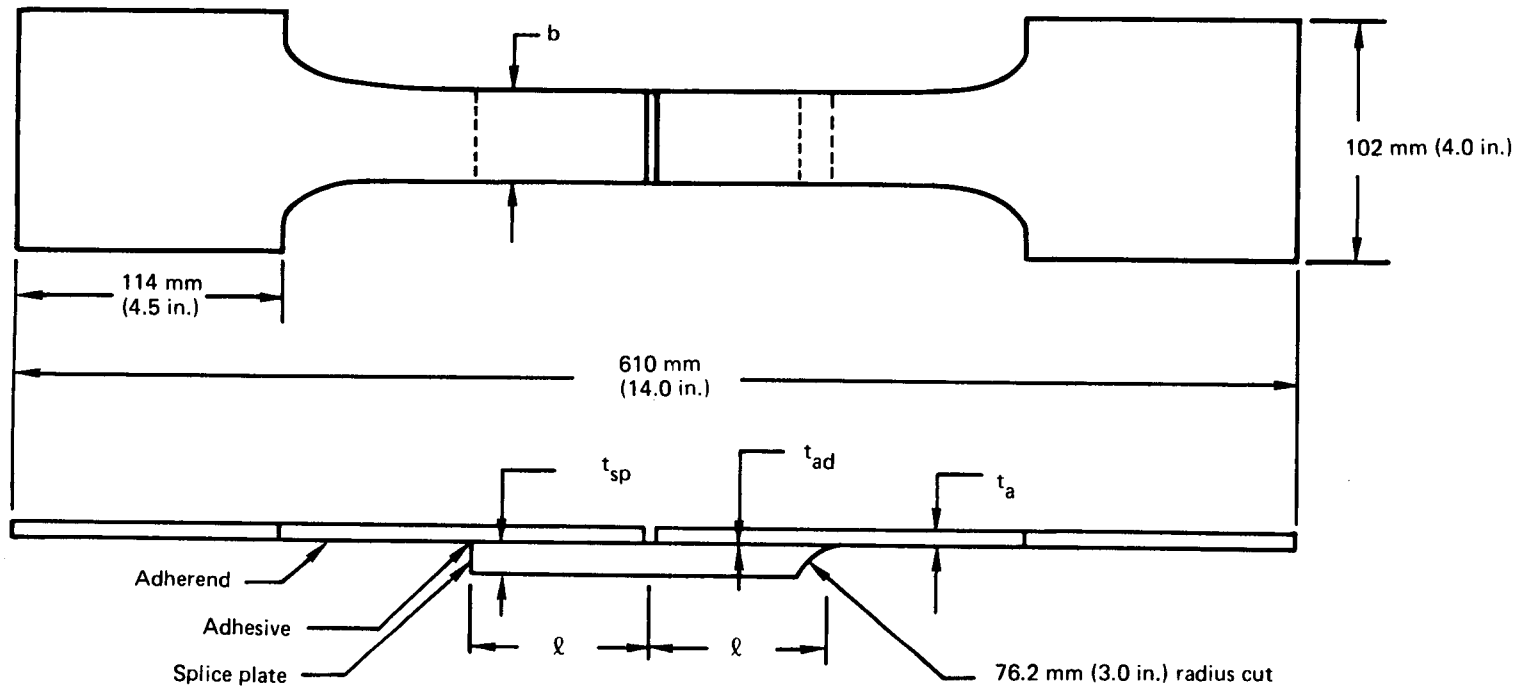

FIGURE 3.–INITIAL TEST SPECIMEN DESIGN

TEST SPECIMEN DESIGN AND FABRICATION

The initial specimen design (fig. 3) consisted of a simple lap splice which required complete load transfer from the adherend through the bondline to the splice plate. A lap length of 127 mm (5.0 in.) was selected as the desired test section. It was deemed desirable to have a single crack begin at one end of the splice plate and propagate the length of the lap to the specimen centerline. To do this it was necessary to have the peak adhesive stress occur at one end of one of the lap lengths. Maintaining a splice plate thickness to adherend thickness ratio greater than 1.0 ensured that the adhesive stresses at the ends of the splice plate exceeded those at the centerline of the specimen. Machining a 76.2 mm (3.0 in.) radius cut into one end of the splice plate provided a transition region and forced the peak stress to occur at the opposite end of the splice plate. A sketch of the assumed relative stress distribution is shown in figure 4. The peak stress in the adhesive occurred at point A at the start of the test and propagated with the adhesive crack front as debonding took place.

The curve used in the flared section simulates the shape that water would take when flowing through a rectangular opening at the base of an infinite reservoir. This curve is defined by a series of coordinates (ref. 6). Since water is incapable of sustaining a shear stress, the water will find the path of least energy in flowing from the reservoir. This means that the shape factor of this curve has a K_t value close to 1.0. The radiused section began 2.5 mm (0.1 in.) beyond the end of the load transfer region under study.

After selecting specific variables for study, an attempt was made to eliminate or at least minimize the effects of other parameters not under investigation. Two such items were batch-to-batch variations in material and day-to-day variations in processing.

Whenever possible, specimens used in this program consisted of materials from the same lot. At the onset of the program a single roll of AF-126 adhesive was obtained. Sufficient pieces of this adhesive film to bond all required AF-126 specimens were cut, individually packaged, and placed in refrigerated storage until required for use. A similar procedure was used with the BP907 laminating resin. One exception to this involved the configuration 4 specimens. They were bonded with production stock adhesive after the storage life recommendations had been exceeded on the original roll of AF-126 adhesive. Instead of using different rolls of adhesive with different nominal thicknesses, the bondline thicknesses required for configurations 2 and 3 were achieved by using multiple plies of the original AF-126 film.

Processing sequences for the titanium/boron-epoxy specimens differed slightly from those used on the aluminum/aluminum specimens. In both cases the sequence of operations minimized the effects of processing variables. Fabrication of the aluminum specimens involved bonding an oversize doubler onto a large, flat sheet. This was done to produce bondlines of controlled uniform thickness. Initially a 1.2 m (48.0 in.) wide by 0.30 m (12.0 in.) long splice plate was bonded to a single piece of adherend stock for each configuration. Subsequent machining operations were then used to produce all of the required test specimens from this single bond assembly. Use of this technique meant that all of the aluminum specimens for any given configuration underwent the same surface preparation, prime, layup, and cure operations.

The specimen planform shape and grip hole pattern were produced by a programmed tape controlled router to ensure uniformity to all specimens. Figure 5 shows a configuration 6 specimen being routed to shape. Additional machine cuts were then used to remove approximately 25.4 mm (1.0 in.) from each end of the splice plate because this region normally contains a tapered bondline due to what is known as the "pinchoff" phenomenon. A final machine cut parted the adherend to produce the load transfer specimen. The resultant lap length for all of the aluminum specimens was 127 mm (5.0 in.).

Fabrication procedures for the titanium/boron-epoxy specimens (configurations 8 and 9) differed from those used on the aluminum/aluminum specimens. The titanium adherend details were first stack routed to the planform shape. At the same time, long lengths of the boron-epoxy composite were laid up and cured to the correct width. These pieces were then machined to lengths ranging from 147 mm (5.8 in.) to 150 mm (5.9 in.). These two details were then bonded together with different bonding agents. The configuration 9 specimens used 12 plies of precured composite and were joined to the titanium with a 13th ply of uncured boron-epoxy. The configuration 10 specimens used 13 plies of precured composite and were joined to the titanium with a single ply of the BP907 laminating resin. These procedures were designed to eliminate the need for machining the composite and titanium at the same time (e.g., the planform shape) and to eliminate waste of the relatively expensive boron composite. The procedures employed meant that all of the titanium/boron-epoxy specimens underwent surface preparation, prime, layup, and cure at the same time.

Initial fatigue tests resulted in adherend failure at the radiused end of the splice plate. The radius cut did eliminate debonding at this point and, in all cases, debonding did begin at the prime crack start location (point A in fig. 4). Unfortunately, the adherend failure consistently took place before the bondline crack propagated to complete failure. To overcome this, the specimens already fabricated as shown in figure 3 were modified to the design shown in figure 6. This consisted of simply shortening the specimen by removing 254 mm (10.0 in.) from the end of the specimen that had been resulting in base metal failure. It also involved adding new grip holes to the 38.1 mm (1.50 in.) wide "stub." Specimens not yet fabricated when the change was made were fabricated directly to the configuration shown in figure 6. Some of the early static specimens were tested in the full dogbone configuration. All of the valid fatigue tests and approximately half of the static tests were tested in the modified "half dogbone" configuration shown in figure 6. Figure 7 shows three completed specimens ready for test.

Additional details of test specimen materials and fabrication procedures can be found in appendixes B and C, respectively.

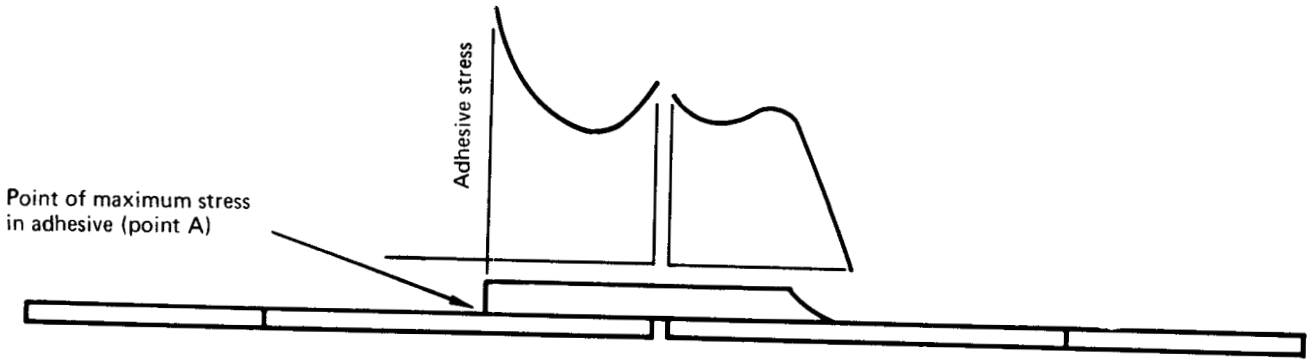

FIGURE 4.—ASSUMED RELATIVE STRESS DISTRIBUTION

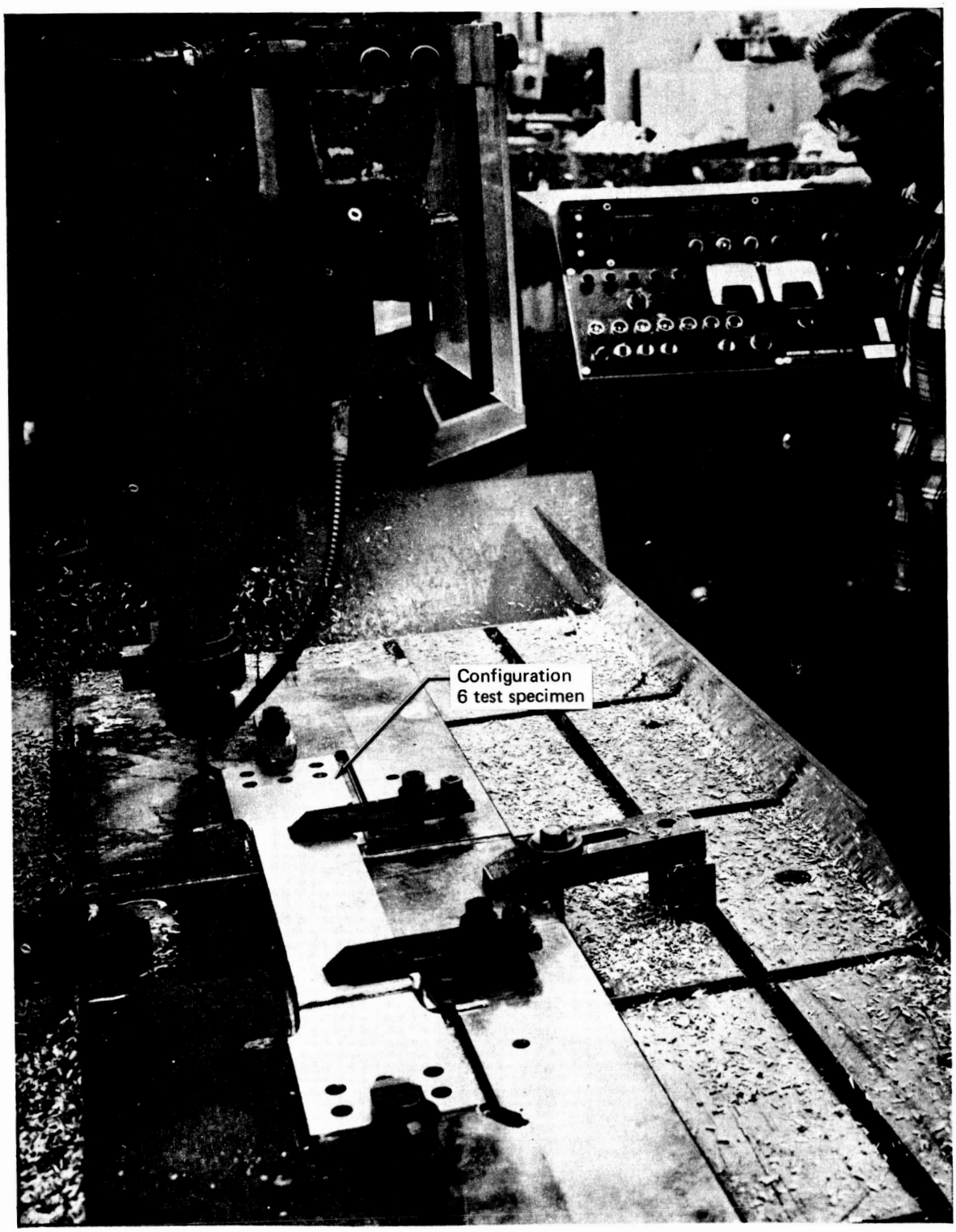

FIGURE 5.–NUMERICAL CONTROL MACHINING OF TEST SPECIMENS

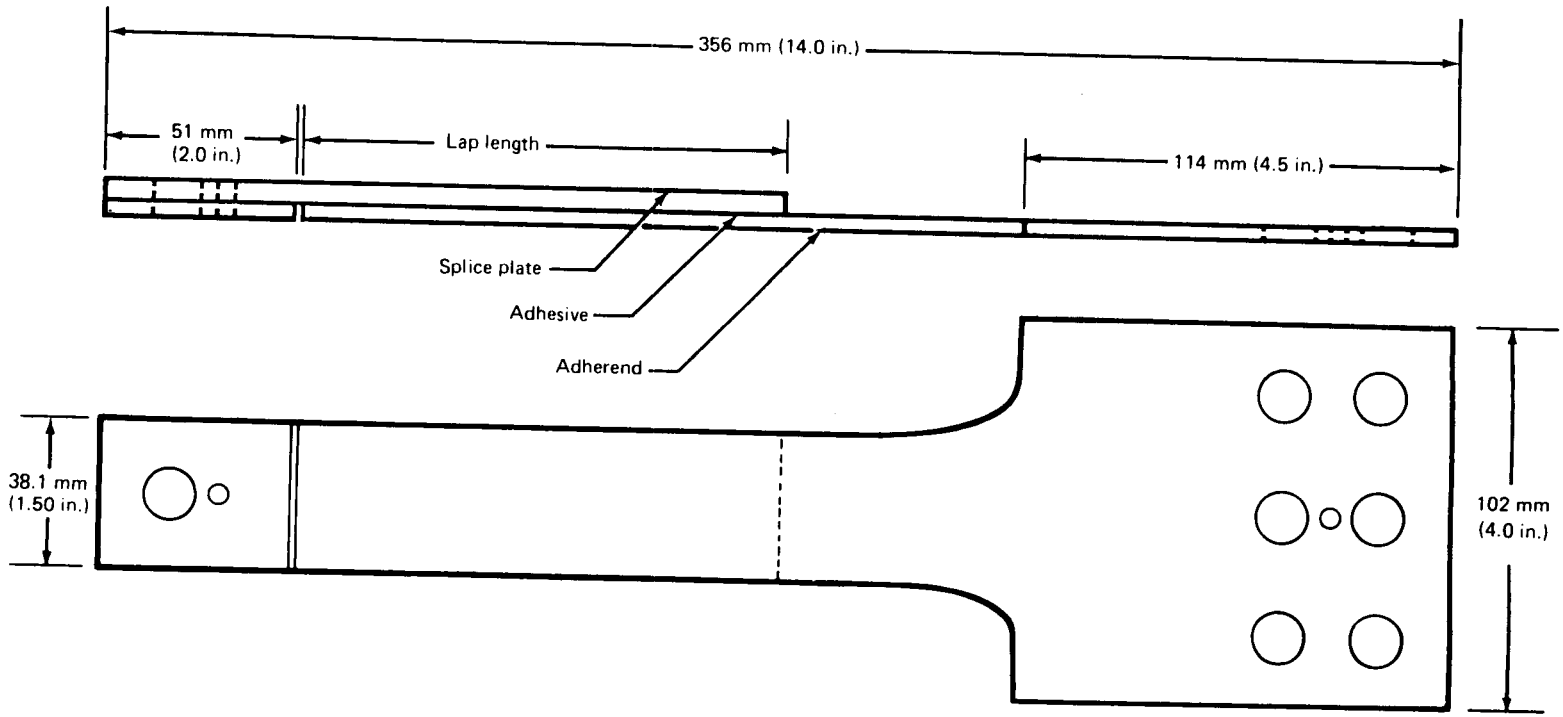

FIGURE 6.–MODIFIED TEST SPECIMEN DESIGN

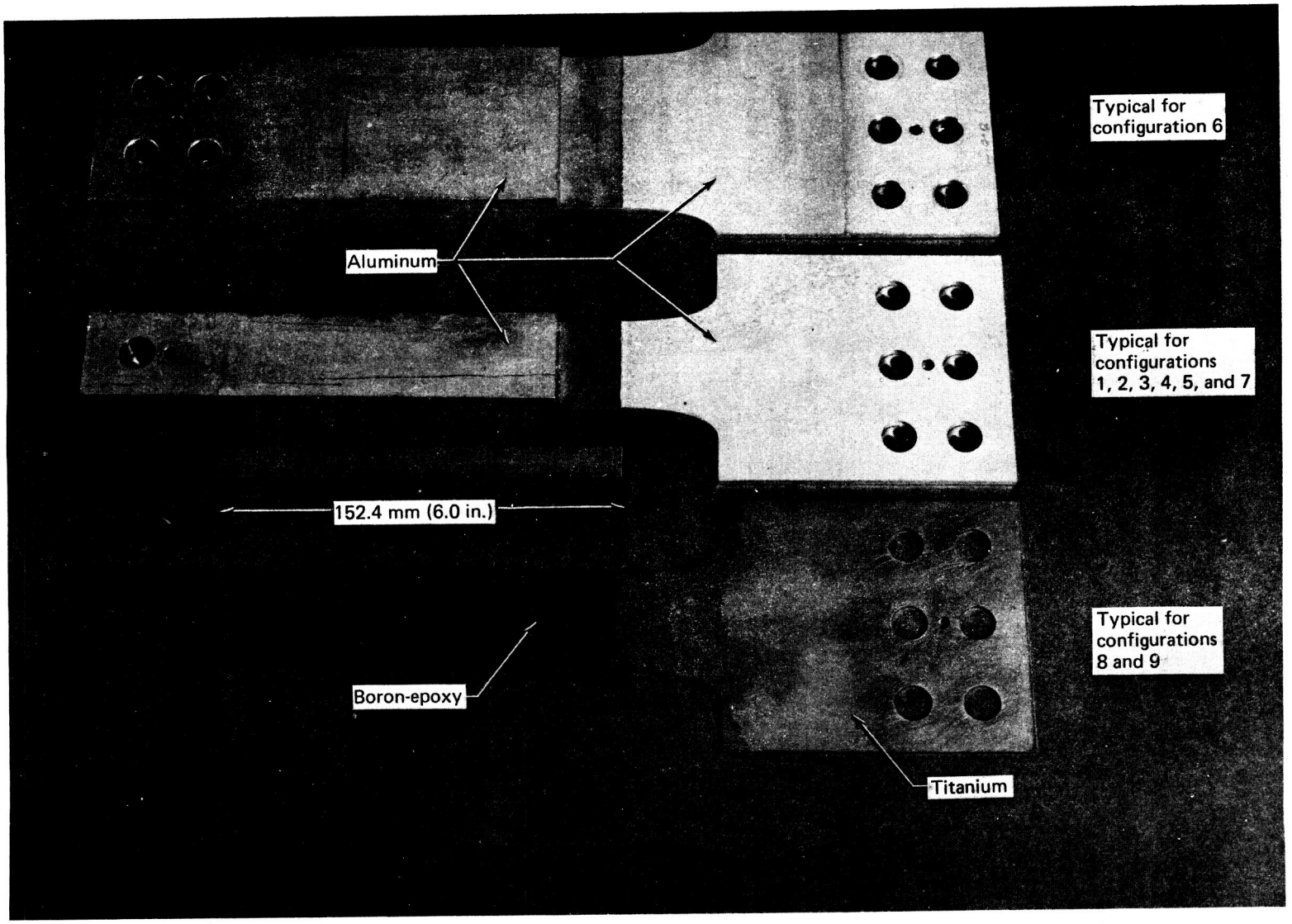

FIGURE 7.–CYCLIC DEBONDING TEST SPECIMENS

TEST PROCEDURE

Static Tests

Static specimens were tested in Baldwin Universal test machines using integral friction head grips on the 610 mm (24.0 in.) long specimens and bolted friction grips on the 356 mm (14.0 in.) long specimens. No lateral restraint was used with any of the static specimens.

All tests were conducted in ambient laboratory environment. Test temperatures ranged from 296°K (73°F) to 302°K (84°F) with an average temperature of 297°K (75°F).

Specimens were loaded continuously to failure at a crosshead deflection rate of 1.27 mm/min (0.05 in./min). A PD-1M extensometer was used to measure head travel deflection. Head travel deflection as a function of load was recorded on an autographic recorder. A photograph of the static test setup is shown in figure 8.

Fatigue Tests

Fatigue tests were performed in Weideman Baldwin SF-10-U fatigue machines operating at 1800 cycles per minute. A stress ratio R = +0.05 was used for all tests. The calculated test loads were initially set on the test machine and then verified by an external load cell. The load cell was then used to monitor the loads for the duration of the test. The SF-10-U test machines used on this program are periodically calibrated to ASTM Designation E-4. Accuracy of load is ±2%. The load cell is also periodically calibrated. Its accuracy is ±1% of load or 89 N (20 lb), whichever is greater. A standard 2:1 load multiplier was used to test the 76.2 mm (3.0 in.) wide specimens and some of the configuration 5 specimens. Least cycle count was 1000 cycles.

Fatigue tests were conducted in ambient laboratory environment. Test temperatures ranged from 294°K (70°F) to 300°K (80°F) with an average temperature of 297°K (74°F). Relative humidity ranged from 14% to 68% and averaged slightly over 30%.

The load was applied through friction at the grip ends. Shims were used to ensure that the centerline of load was coincident with the centerline of bond. No lateral restraint was used with this test setup.

Immediately prior to testing, an adhesive-backed scale was fixed to each side of the specimen splice plate. Debond lengths were obtained by stopping the alternating load, applying a light coat of fluorescent dye penetrant to the edges of the specimen, wiping clean, and then reading the crack length directly with the aid of a hand-held ultraviolet light. Readings were taken on both edges of the specimen. Reading interval was established by the test engineer during the test. Low debond rates were monitored at intervals of several thousand cycles, whereas high rates of debonding were monitored at 1000-cycle or shorter intervals. Final cycles to failure or readings at less than 1000-cycle intervals were estimated by timing the load application interval. Accuracy of debond length measurements is believed to be ±0.25 mm (±0.01 in.).

The titanium/boron-epoxy specimens were tested with the as-bonded splice plate length; however, only the last 127 mm (5.0 in.) were considered for data analysis.

Figure 9 shows a typical fatigue test setup and figure 10 shows a debond length reading being made. Figure 11 shows a failed fatigue specimen taken with the aid of an ultraviolet light. This photo shows the permanent record left by the dye penetrant after various numbers of cycles.

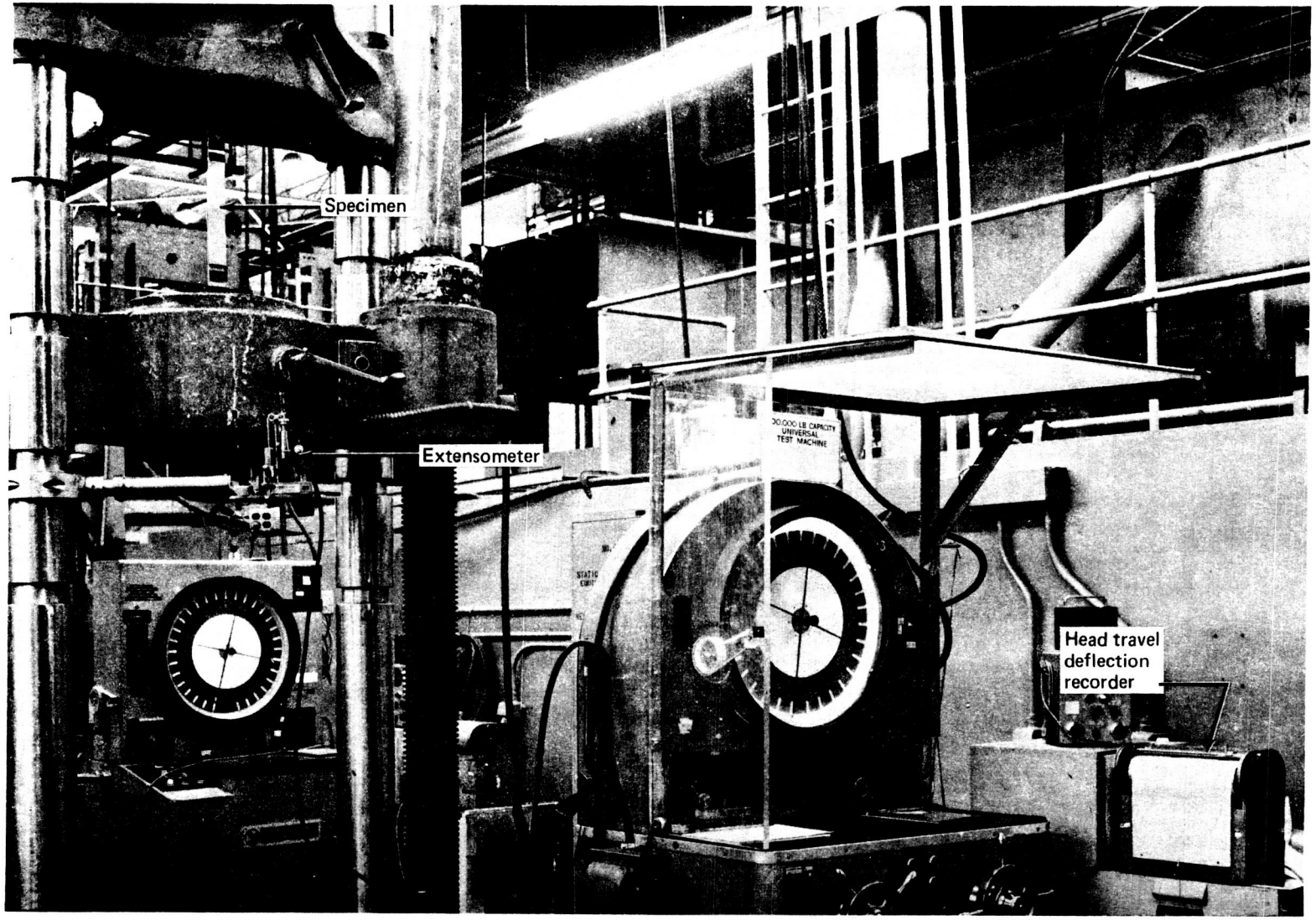

FIGURE 8.–STATIC TEST SETUP

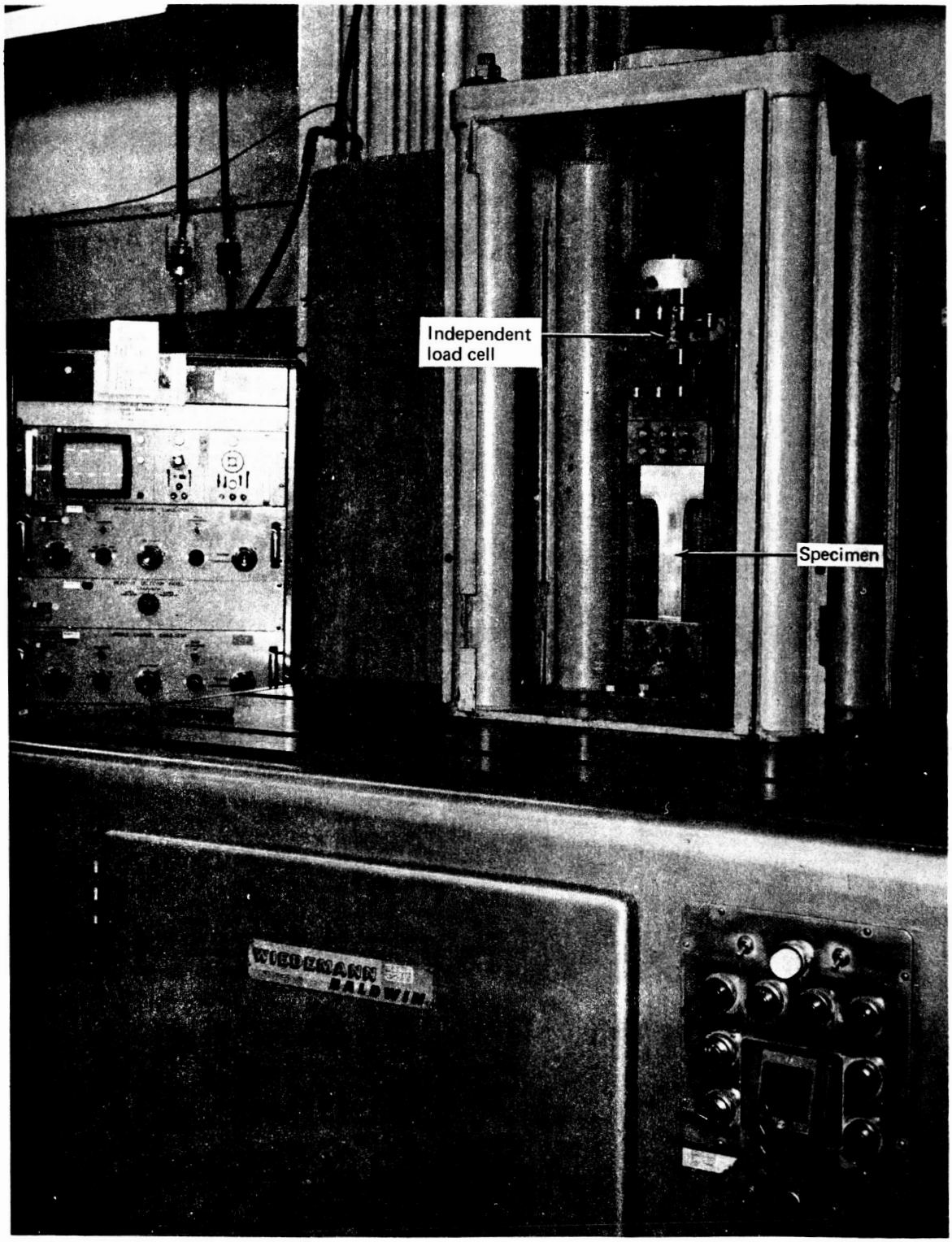

FIGURE 9.—FATIGUE TEST SETUP

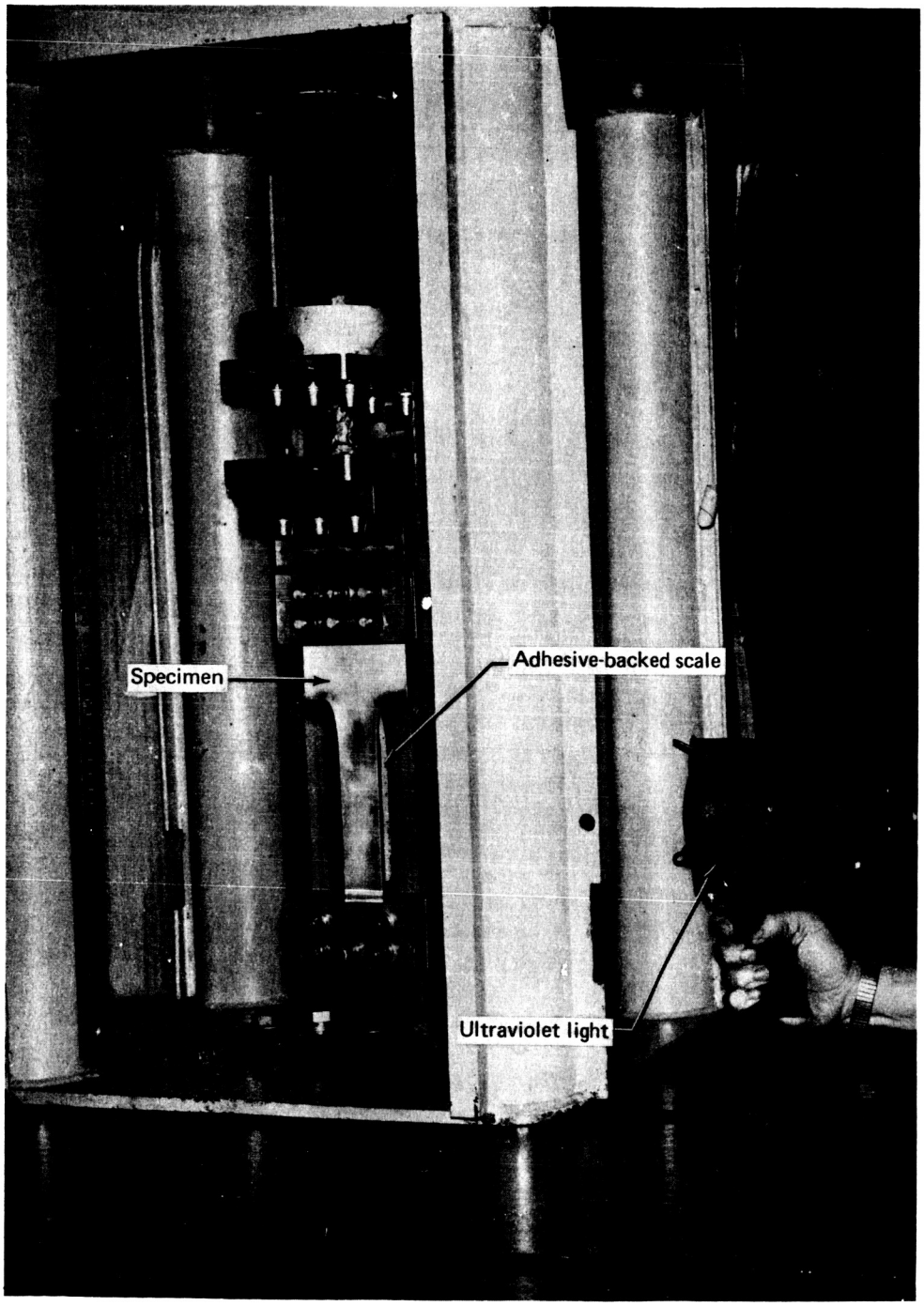

FIGURE 10.–DEBOND READING TECHNIQUE USING ULTRAVIOLET LIGHT

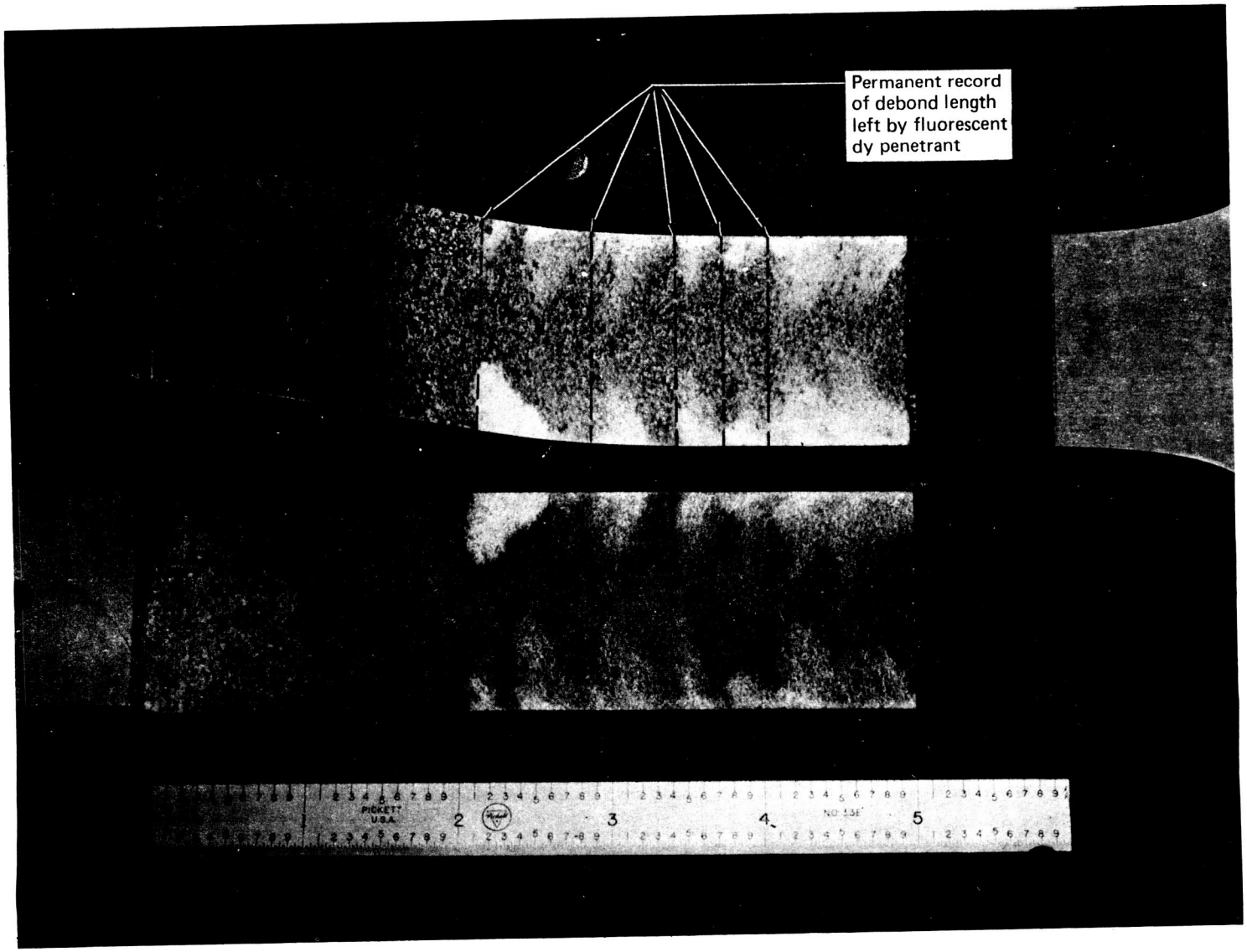

FIGURE 11.–FAILED FATIGUE SPECIMEN SHOWING DEBOND LENGTH RECORD

TEST RESULTS AND DISCUSSION OF RESULTS

Static Tests

Static test results are summarized in table 2. The static specimens were identified by an alphanumeric character consisting of the configuration number followed by the letter "S" and a number to designate replicate specimens. For example:

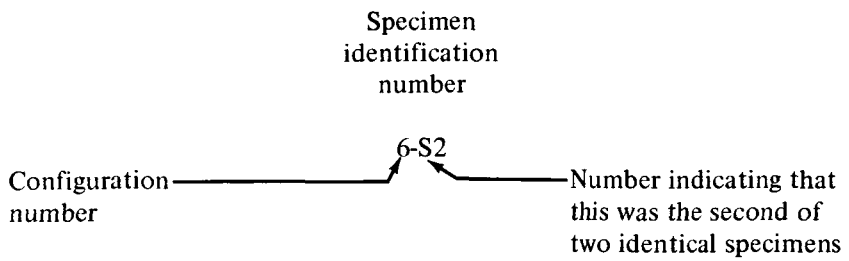

Results are summarized in terms of ultimate load and the maximum gross area tensile stress in the adherend (assuming no contribution for bending). With one exception, all static test specimens failed cohesively. After partial cohesive debonding, specimen 9-S2 failed in the boron-epoxy splice plate.

Configurations 1 through 6 used the AF-126 adhesive system. These specimens began debonding from the end of the splice plate when the adherend stresses at that point were above F_{ty}. The crack in the bondline traveled slowly at first, accompanied by considerable yielding in the adherend. The debond rate increased noticeably when the crack length had grown to approximately 38.1 mm (1.5 in.). Thereafter, the debond rate continued to accelerate, eventually reaching a point where the test machine could not maintain its load on the specimen.

Examination of the failed specimens revealed that the failure plane within the adhesive lay closest to the more highly strained piece of metal. This meant that at the beginning of the test and for the majority of the lap length, the failure plane was closer to the adherend than the splice plate. A short length near the stub end had the failure plane closer to the splice plate. This results in a banded failure surface as shown in figure 12. Also visible in this photograph is the elongation of the adherend.

Configurations 1 through 6 all developed stresses in the adherend near tensile ultimate. Because the strengths shown in table 2 are approaching a limiting value (i.e., ultimate metal strength), they do not show the strength variation between configurations that might have been obtained with shorter lap lengths. Some trends in the results are evident. Configuration 1 specimens had a 0.1016 mm (0.004 in.) thick bondline. Configuration 2 specimens had a 0.2540 mm (0.010 in.) thick bondline and showed a definite increase in strength. Configuration 3 specimens had a 0.4064 mm (0.016 in.) thick bondline. These specimens showed only a negligible increase in strength when compared to the specimens with medium thickness bondlines. The configuration 6 specimens had a test section width of 76.2 mm (3.0 in.). These specimens showed virtually the same static strength as the configuration 1

specimens that had the standard 38.1 mm (1.5 in.) width. Configuration 5 specimens used a heavier adherend gage and a lighter splice gage than configuration 1 specimens. The slight increase in strength is due to a slight decrease in load path eccentricity. Configuration 4 specimens used a lighter splice plate gage than the configuration 1 specimens. A slight increase in strength is noted, at least a portion of which is due to a decrease in load path eccentricity. It should also be noted that the adhesive used for the configuration 4 specimens came from a different batch than that used for configuration 1. Some batch-to-batch variation in strength could be expected. This set of specimens was tested in the 356 mm (14.0 in.) long configuration, and all other AF-126 specimens were tested in the 610 mm (24.0 in.) long full-dogbone configuration; however, the configuration change was not believed to have influenced test results.

Configurations 7, 8, and 9 used the BP907 laminating resin as an adhesive. The configuration 7 specimens used aluminum adherends and splice plates. The configuration 8 and 9 specimens used titanium adherends and boron-epoxy splice plates. These specimens gave generally lower static strengths than the specimens bonded with AF-126 adhesive. This is a result of the different stress-strain characteristics of the two systems. Although the BP907 system has been shown to have both higher strength and modulus than the AF-126 system, the AF-126 system had approximately 10 times the ultimate elongation capability of the BP907 system. All of the BP907 specimens failed with little or no yielding of the adherends. Also, debonding and failure took place in less time than for the specimens bonded with AF-126 adhesive.

The effects of the material property differences between the AF-126 and BP907 systems are illustrated in figure 13. This figure contains typical static test load deflection curves for four configurations. All four configurations were tested with the modified specimen shape shown in figure 6. The configuration 4 specimens used AF-126 adhesive with aluminum adherends and splice plates. This configuration displays considerably more elongation than the other three. Although the deflection shown in figure 13 is primarily a result of the adherend yielding in the lap area, the ability of the AF-126 system to carry load in a joint having adherend stresses above yield is evident.

Configuration 7 used the BP907 laminating resin with aluminum adherends and splice plates. Configurations 8 and 9 were the titanium/boron-epoxy combinations and also used the BP907 system. Very little inelastic deformation capability was observed with these specimens. Once initiated, failure took place rapidly. The inability of the BP907 system to sustain large elongation was expected to and did influence the debonding results.

Fatigue Tests

Reference 1 contains individual test specimen logs for all 106 fatigue specimens. All of these specimens were tested in the modified configuration shown in figure 6, and all except five resulted in cohesive debond failure. These five specimens exhibited partial cohesive debonding but eventually resulted in adherend or splice plate failure.

It became apparent during the fourth month of testing that there was a definite change in behavior with some of the AF-126 specimens. Data that had been produced in the first and second months of testing could not be reproduced in the fourth month. This discrepancy affected configurations 1, 2, 3, 5, and 6. Configurations 1, 2, 3, and 5 showed shorter lives in the fourth month than they had earlier. Configuration 6 specimens reversed this trend and showed longer lives at the later date. A review of the test procedures was begun late in the fourth month of testing to try to isolate the reason for the behavior change.

Environmental degradation did not seem likely. The majority of the test specimens were stored in the fatigue test laboratory prior to test. Some specimens, however, were machined shortly before test from excess bond assembly stock that had been stored in the bond shop prior to machining. A comparison of specimens stored in both places showed no apparent difference in the aging effect. It seems unlikely that specimens stored in two different places would have been exposed to and affected by the same adverse environment. Another argument against environmental degradation is that this type of damage normally results in an adhesively failed surface. All of the specimens involved here failed cohesively.

During the peak testing periods, several SF-10-U fatigue machines were being used. A check of the machine logs showed that the aging phenomenon was not limited to any particular machine.

An examination of the failed specimens revealed that the amount of dye penetrant applied to individual specimens varied considerably. This variation, however, was random in nature and definitely not related to test date or age of the specimen. It was also determined that the amount of residual dye penetrant remaining on the specimen was not related to specimen life. Some specimens with a considerable amount of residual dye penetrant had the longest life of the three replicate specimens, while in other cases they had the shortest life.

The possibility that test results might have been highly sensitive to test specimen installation and shimming procedures was also investigated. This did not prove to be the case. The shims used to locate the specimens were continually being replaced due to damage suffered when the specimens failed. Had the test results been highly sensitive to the shimming and installation procedure, they should have exhibited a generally high degree of scatter. In actuality, the scatter of tests run in the same time period was relatively small. As an additional check, two extra configuration 3 specimens were tested late in the fourth month of testing. One of these specimens was tested with the shims intentionally mislocated to place the centerline of load application along the centerline of the adherend. The other specimen was tested with the shims correctly located. These two specimens gave lives of 7.3 and 8.5 kc, respectively. Three identical specimens tested at the same stress level 70 days earlier had given lives of 12.2, 13.0, and 12.8 kc. It appeared that the test setup had a minor effect when compared to the effect of the additional 70 days that elapsed between the two sets of tests.

Configurations 4, 7, 8, and 9 did not appear to vary with time. Configuration 4 used the AF-126 system; however, the adhesive was taken from a different batch than that used for configurations 1, 2, 3, 5, and 6. Configurations 7, 8, and 9 used the BP907 laminating

resins as an adhesive. It should also be noted that the specimens for configurations 4, 7, 8, and 9 were all tested at a considerably earlier age and with less time spread than the specimens involved in configurations 1, 2, 3, 5, and 6.

No logical explanation was found for the time-dependent behavior. This should definitely be a subject for additional investigation.

Typical curves of crack length as a function of cycles for each configuration are shown in figures 14 through 22. The curves are labeled with the number of specimens used, the maximum applied stress in the adherend, and the approximate number of days after cure (DAC) that the test took place. The exact number of days after cure for each specimen is shown in reference 1. Wherever the apparent time dependency effect was observed the data have been shown as a solid line for specimens tested in one time period and a dashed line for specimens tested in the other time period.

In cases where only one specimen was used to generate the curve, a smooth line was drawn through the data points for that specimen. Where two or more specimens were involved, the life shown is the arithmetic average for the specimens involved. The critical crack length (i.e., the point where the curve has an infinite slope) was established by examining the failed specimen. The portion of the curve from zero crack length to critical crack length was drawn as a best interpretation of the available data points.

The specimens for configurations 8 and 9 were tested with lap lengths ranging from 147 mm (5.8 in.) to 150 mm (5.9 in.). To coincide with the other configurations, however, only the last 127 mm (5.0 in.) were used to produce the summary curves shown in figures 21 and 22.

The fatigue specimens showed generally good reproducibility regarding time to failure. Figures 14 through 22 show a life range for individual groups of specimens. In general, longer average life was accompanied by greater scatter, and the specimens bonded with the AF-126 adhesive system showed less scatter than those bonded with the BP907 system.

It had been anticipated that the cyclic debonding specimens would show crack growth rate as a function of crack length behavior similar to that shown in figure 23. With a long lap length, some amount of constant crack extension per cycle was expected during the first part of the test. It was also expected that this uniform growth rate would be followed by a region of accelerating growth rate. As the crack length increased (i.e., the remaining bond area decreased), the increasing shear stress in the bond was expected to cause the increase in the crack growth rate.

Figures 24 through 32 show typical crack growth rates as a function of crack length for each configuration. These plots were generated by taking slopes at various crack lengths from the curves shown in figures 14 through 22. Again data are shown as a solid line for one time range and a dashed line for a second time range wherever applicable. It can be seen that many of the curves follow the shape suggested in figure 23. Several other curves exhibit an increasing or decreasing rate at first and then settle into a constant rate of debonding prior to the onset of rapid debonding and failure. Normally this variation worked itself out in the first 25.4 mm (1.0 in.) of debonding. The main exception in this behavior occurred for

configuration 1. The debond rate for these specimens slowed as the crack length increased. This trend continued until the onset of rapid debonding and failure. Additional research is necessary to resolve this behavior.

For those configurations where data varied with the age of the test specimen, the initial debond rate of the shorter lived specimens is equal to or somewhat greater than the rate experienced by their longer lived counterparts. The big difference is that those specimens having shorter lives show an accelerating debond rate with shorter crack lengths and fail with shorter critical crack lengths.

Figure 33 shows debond rates as a function of maximum initial average bond shear stress. This stress is based on the maximum applied fatigue load divided by the lap bond area for a 127 mm (5.0 in.) lap. The debond rates used in these curves were the constant rate portions prior to the onset of rapid debonding and failure. For some specimens this is the original rate; for others it is the rate achieved after about 25.4 mm (1.0 in.) has been debonded. Data are shown for configuration 1 even though no region of linear debonding was observed. These points were obtained by taking approximate slopes from the curves shown in figure 13. Also, it should be noted that no time effect is shown on this figure. Where data varied with the age of the specimen, data are shown only for the time period with the lower debond rates.

This figure gives an indication of how various configurations resisted debonding for the early constant growth rate portion of the test. Generally the data fall into two groups: one contains the three configurations bonded with BP907 laminating resin (configurations 7, 8, and 9), and the other contains the specimens bonded with the AF-126 adhesive (configurations 1-6). As had been expected from the static test results, the specimens bonded with the AF-126 adhesive resisted debonding better than those bonded with the BP907 laminating resin.

Configurations 1, 2, and 3 involved the study of bondline thickness. Specimens with the medium thickness bondlines clearly outperformed both those having thin and those having thick bondlines. It would appear that an optimum bondline thickness exists above and below which fatigue resistance is reduced.

The configuration 4 specimens used a lighter splice plate gage than the configuration 1 baseline specimens. The configuration 5 specimens used both a heavier adherend gage and a lighter splice plate than the baseline. The configuration 4 and 5 specimens both had lower splice plate thickness to adherend stiffness ratios than the baseline, and both sets of specimens had lower debond rates than the baseline. Although the exact reason for this is unknown, it is reasonable to expect that the average bond shear stress used in figure 33 is an oversimplification of a complex phenomenon. Debond rates will also depend on the amount of load being transferred and the prying load at the end of the lap due to out-of-plane deformation. Exploratory tests had been performed early in the program to determine the most suitable specimen configuration and lateral restraint system. One restraint system placed the specimen between two teflon-lined I-beams. The I-beams were bolted together and, although no clamp-up force was applied, the beams prevented lateral separation of the splice plate from the adherend. This setup was found to drastically reduce the debond rate and strongly suggested that stress components perpendicular to the plane of the bondline

influenced the failure rate early in the test. This restraint system was not used for any additional tests since it was believed to simulate a situation that did not normally exist in actual joints.

The configuration 6 specimens were used to check specimen width. These specimens used a test section width that was twice that of the baseline (configuration 1). The initial debond rates for these two sets of specimens are almost identical, indicating that specimen width does not have a significant effect on debond rate.

Configurations 7, 8, and 9 used the BP907 laminating resin as an adhesive. All three sets of specimens show faster debond rates than the specimens bonded with AF-126 adhesive. The specimens with the aluminum adherends have a considerably slower debond rate than either of the titanium/boron-epoxy specimens. The configuration 8 specimens were co-cured. With this fabrication technique, the resin from the prepreg tape serves as the bonding agent to join the details. These specimens definitely outperformed the configuration 9 specimens that were assembled by a sequential cure. Specimens assembled by the sequential cure method used an extra layer of laminating resin as an adhesive.

TABLE 2.–STATIC TEST RESULTS

Configuration	Specimen identification number	Ultimate load		Ultimate stress in adherend	
		N	lb	MN/m^2	psi
1	1-S1	62 942	14 150	518.94	75 266
	1-S2	62 275	14 000	511.54	74 192
	Avg	62 609	14 075	515.24	74 729
2	2-S1	67 390	15 150	530.77	76 982
	2-S2	67 390	15 150	533.48	77 375
	Avg	67 390	15 150	532.12	77 178
3	3-S1	67 835	15 250	534.54	77 529
	3-S2	68 725	15 450	544.04	78 907
	Avg	68 280	15 350	539.29	78 218
4	4-S1*	64 766	14 560	525.31	76 190
	4-S2*	65 656	14 760	538 44	78 095
	Avg	65 211	14 660	531.88	77 142
5	5-S1	78 955	17 750	533.72	77 410
	5-S2	78 733	17 700	536.19	77 768
	Avg	78 845	17 725	534.95	77 589
6	6-S1	124 772	28 050	517.24	75 020
	6-S2	123 882	27 850	509.47	73 892
	Avg	124 328	27 950	513.36	74 456
7	7-S1*	55 158	12 400	453.31	65 747
	7-S2*	55 425	12 460	450.72	65 372
	Avg	55 291	12 430	452.02	65 560
8	8-S1*	40 968	9 210	694.76	100 766
	8-S2*	39 500	8 880	665.50	96 522
	Avg	40 234	9 045	680.13	98 644
9	9-S1*	34 518	7 760	583.46	84 624
	9-S2*	38 388	8 630	642.56	93 196
	Avg	36 453	8 195	613.01	88 910

*Specimens tested with modified configuration shown in figure 6.

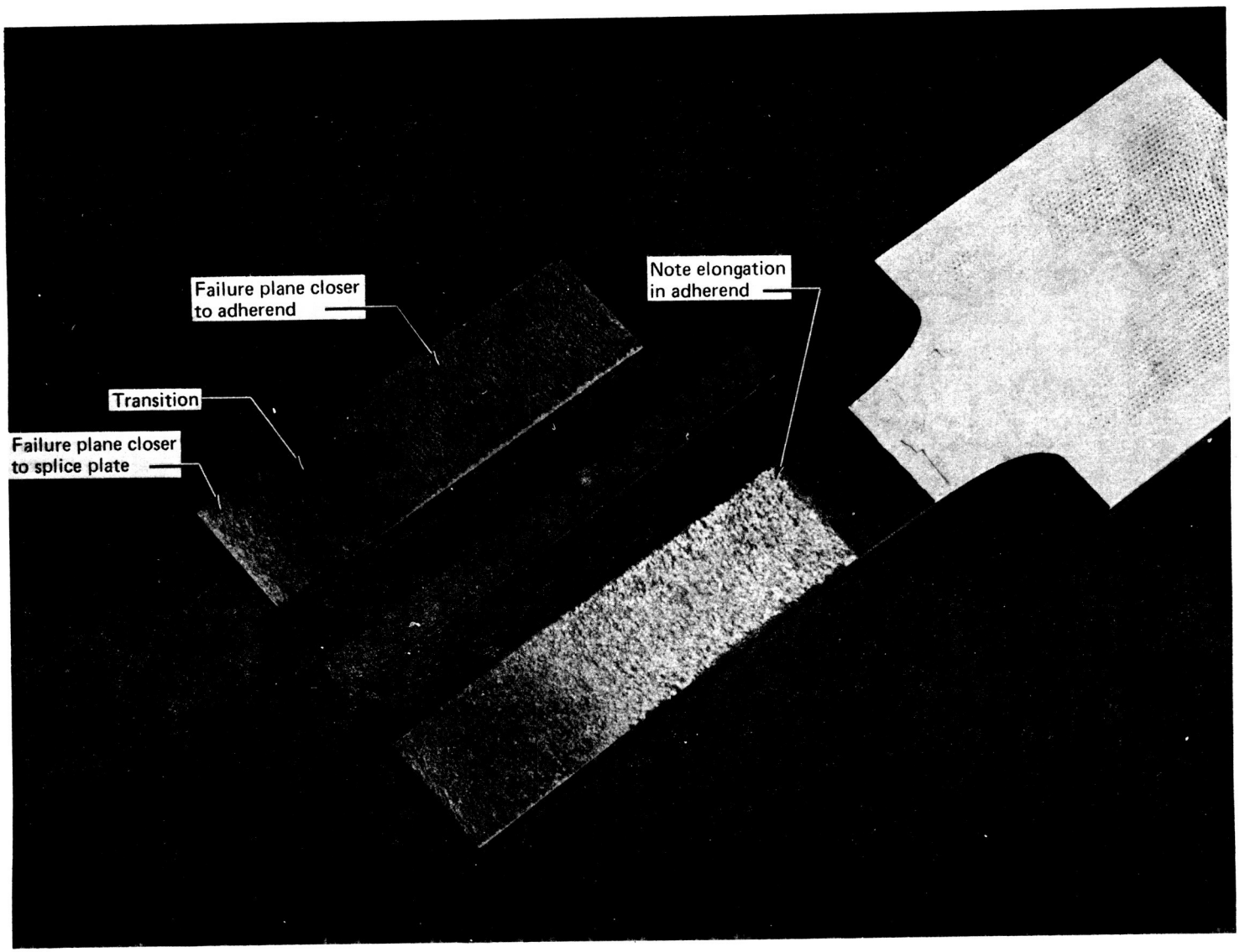

FIGURE 12.—FAILED STATIC SPECIMEN

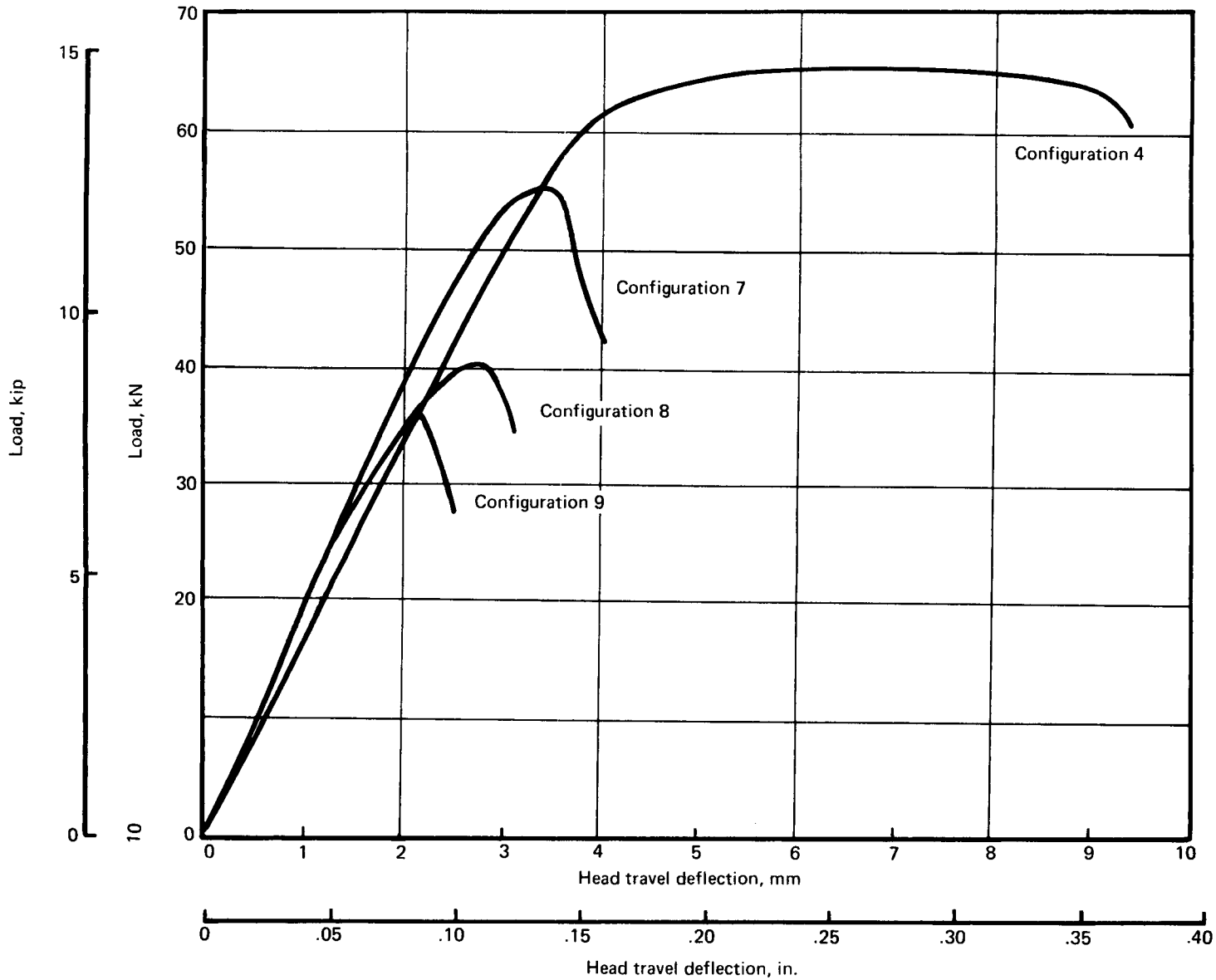

FIGURE 13.–TYPICAL LOAD DEFLECTION CURVES FOR STATIC SPECIMENS

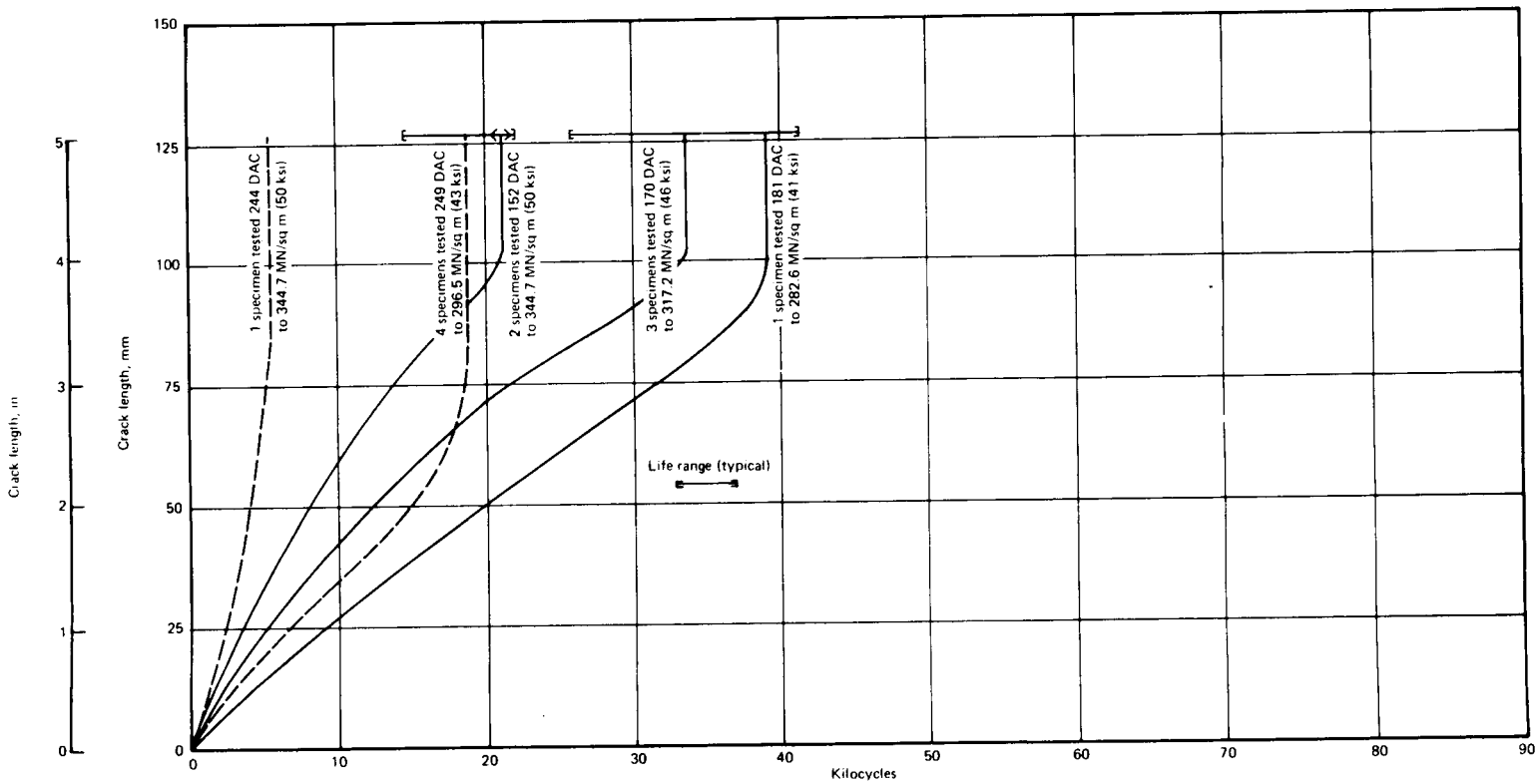

FIGURE 14.–CRACK LENGTH AS A FUNCTION OF CYCLES FOR CONFIGURATION 1

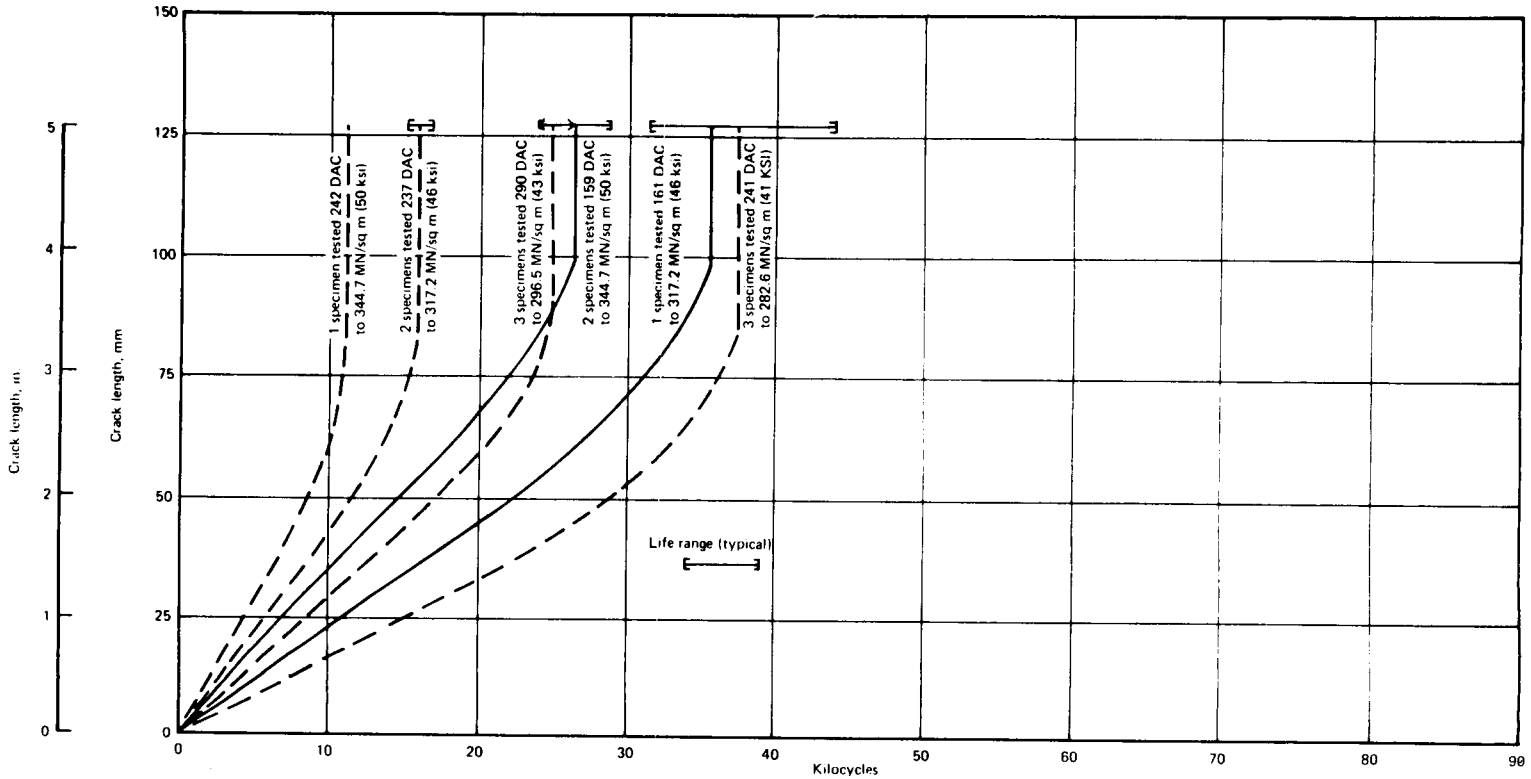

FIGURE 15.—CRACK LENGTH AS A FUNCTION OF CYCLES FOR CONFIGURATION 2

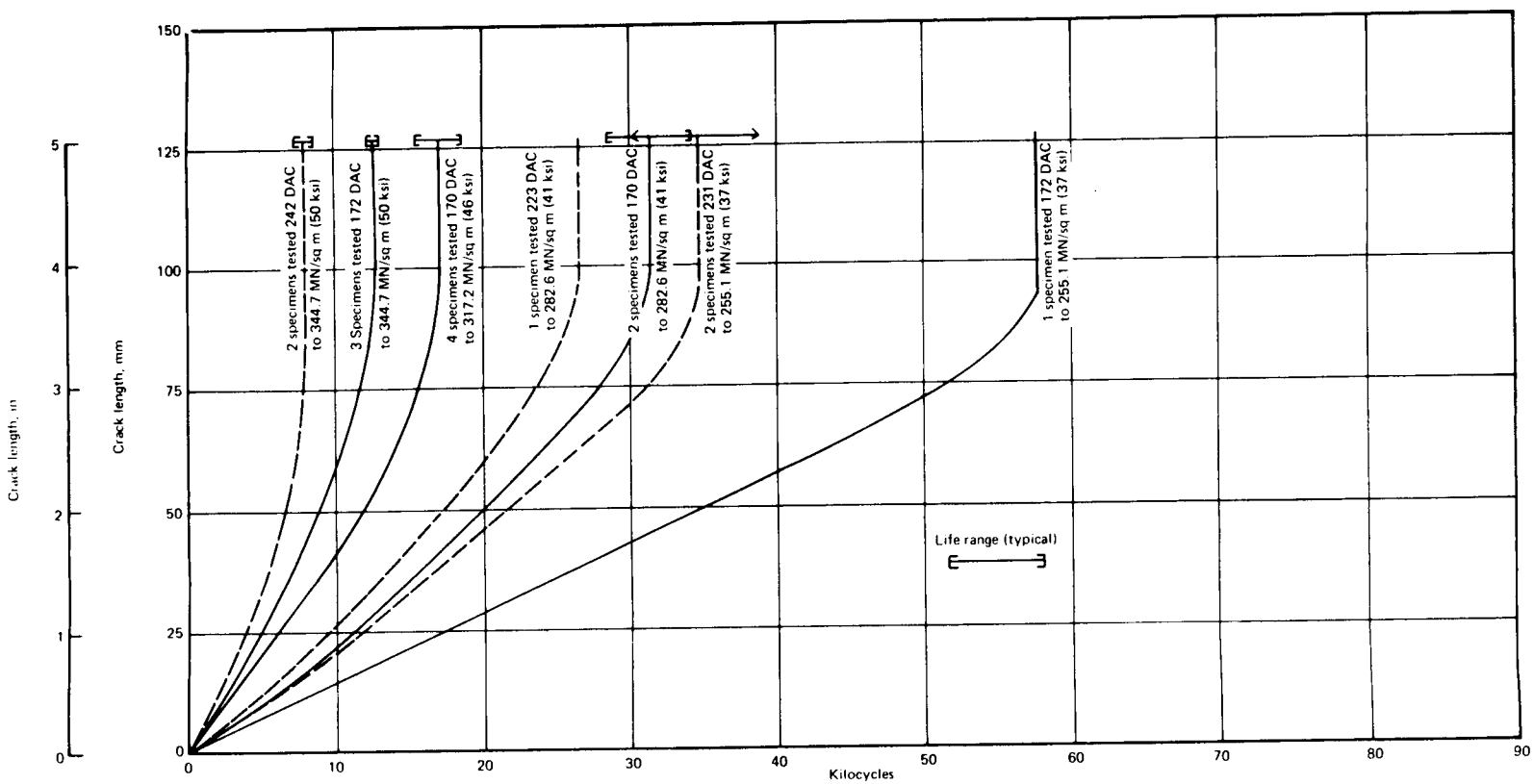

FIGURE 16.–CRACK LENGTH AS A FUNCTION OF CYCLES FOR CONFIGURATION 3

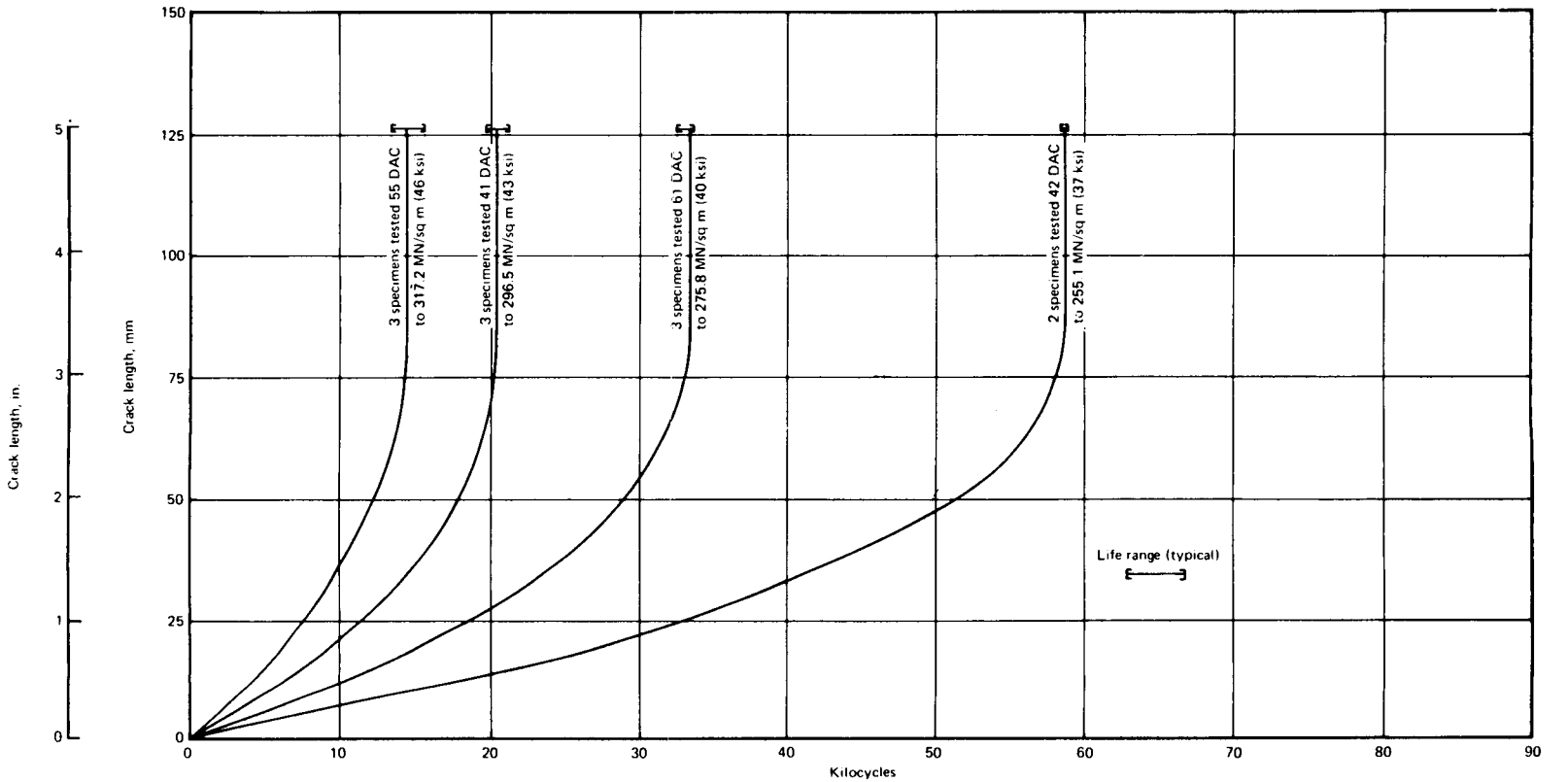

FIGURE 17.–CRACK LENGTH AS A FUNCTION OF CYCLES FOR CONFIGURATION 4

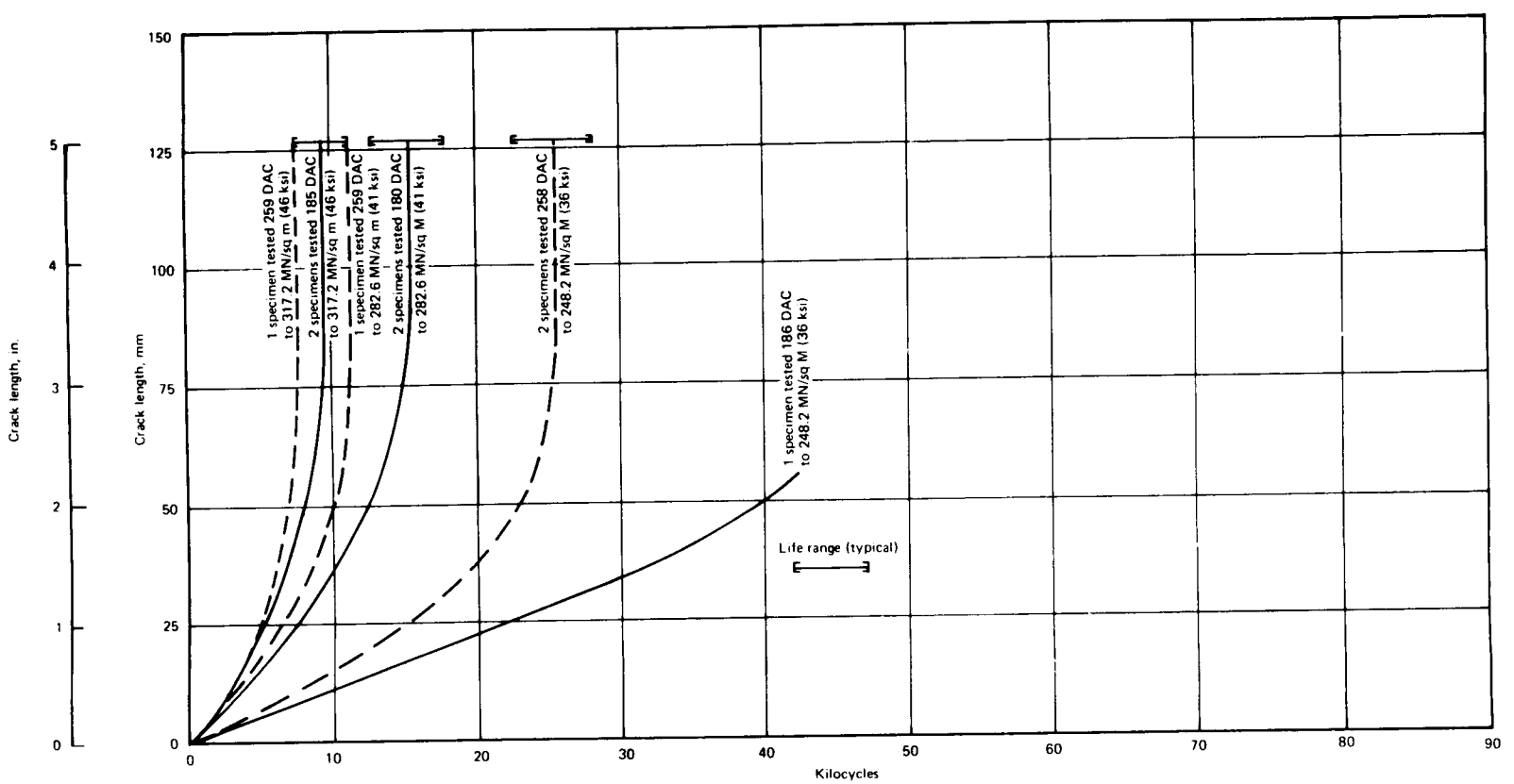

FIGURE 18.—CRACK LENGTH AS A FUNCTION OF CYCLES FOR CONFIGURATION 5

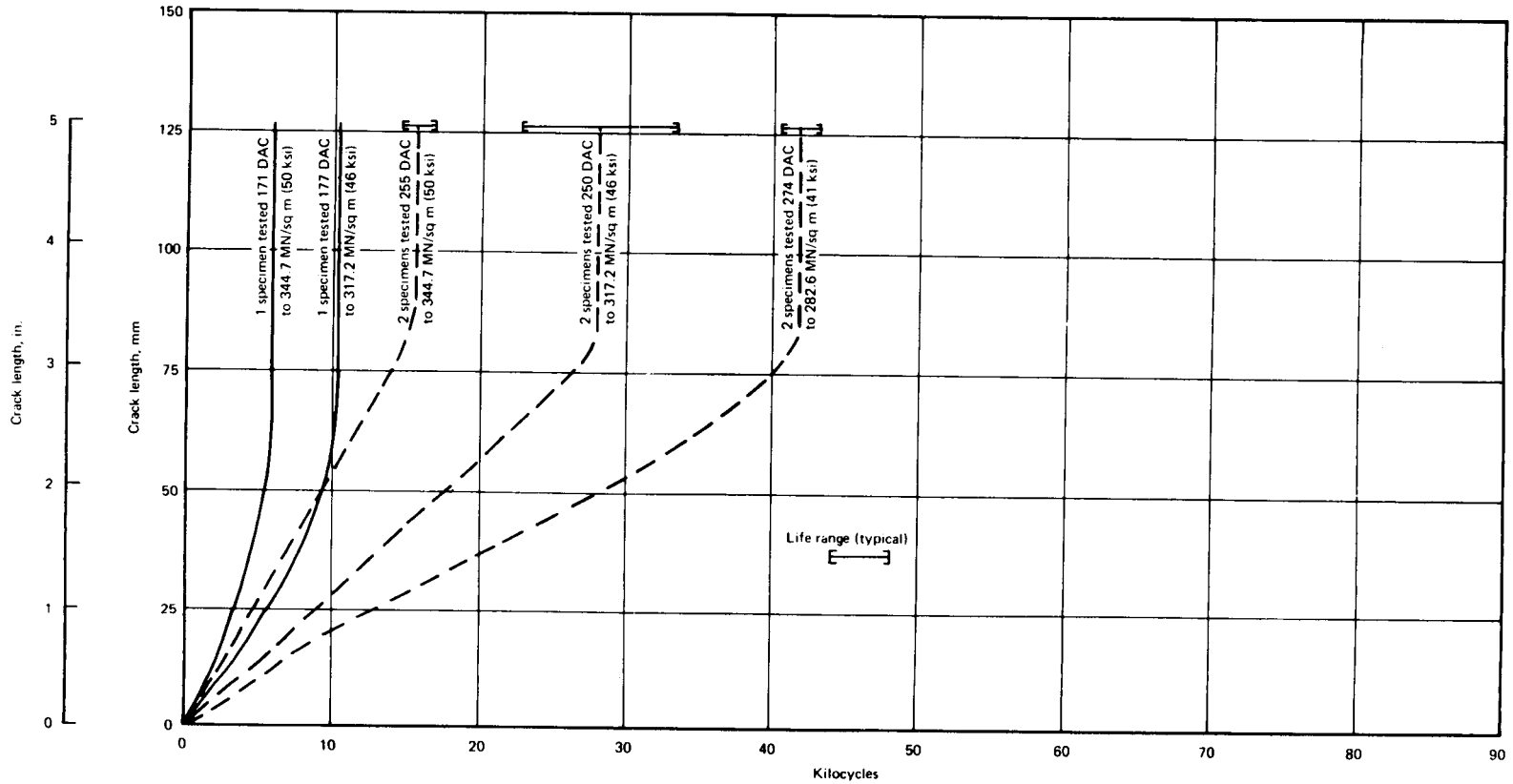

FIGURE 19.—CRACK LENGTH AS A FUNCTION OF CYCLES FOR CONFIGURATION 6

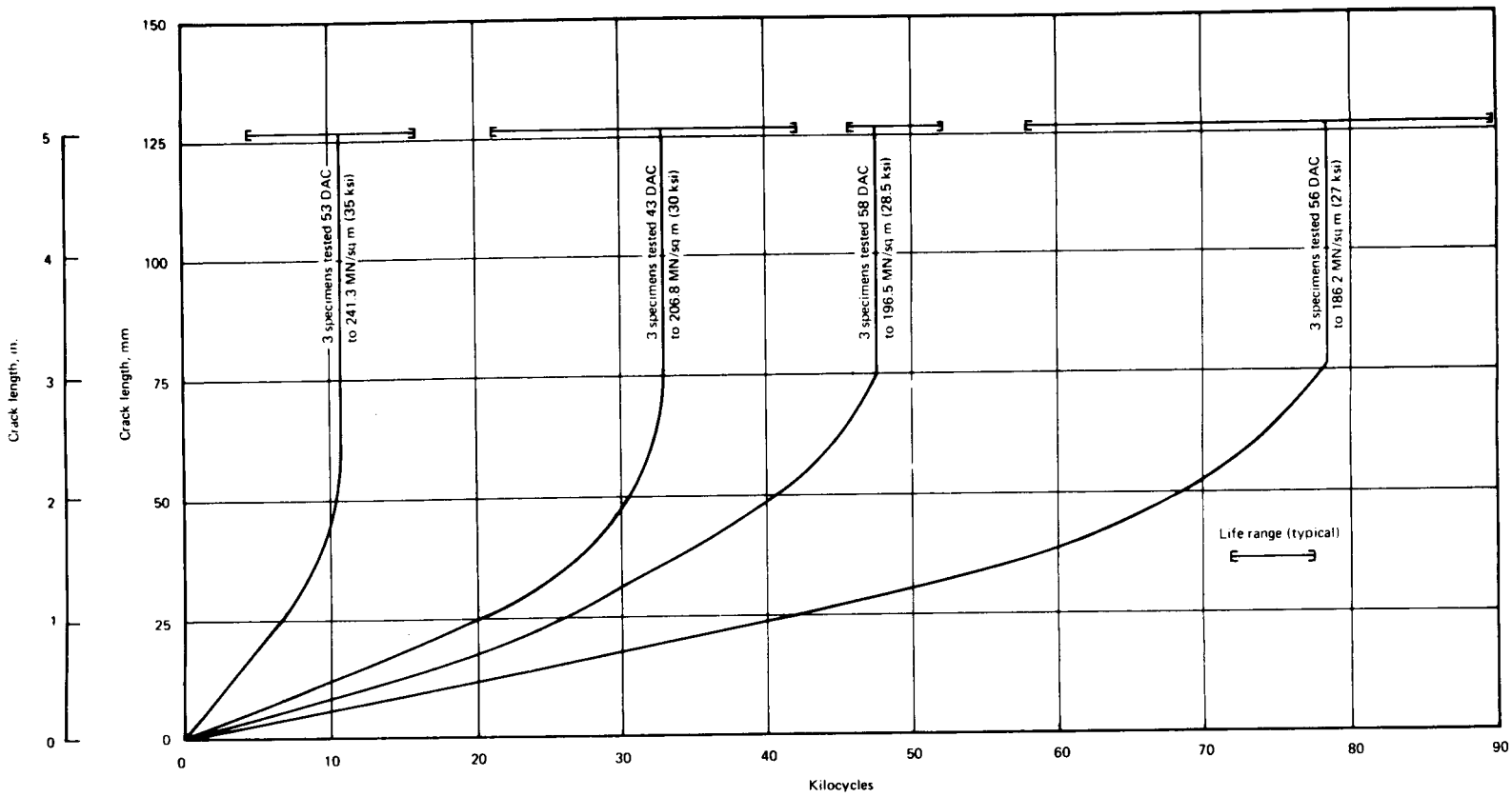

FIGURE 20.–CRACK LENGTH AS A FUNCTION OF CYCLES FOR CONFIGURATION 7

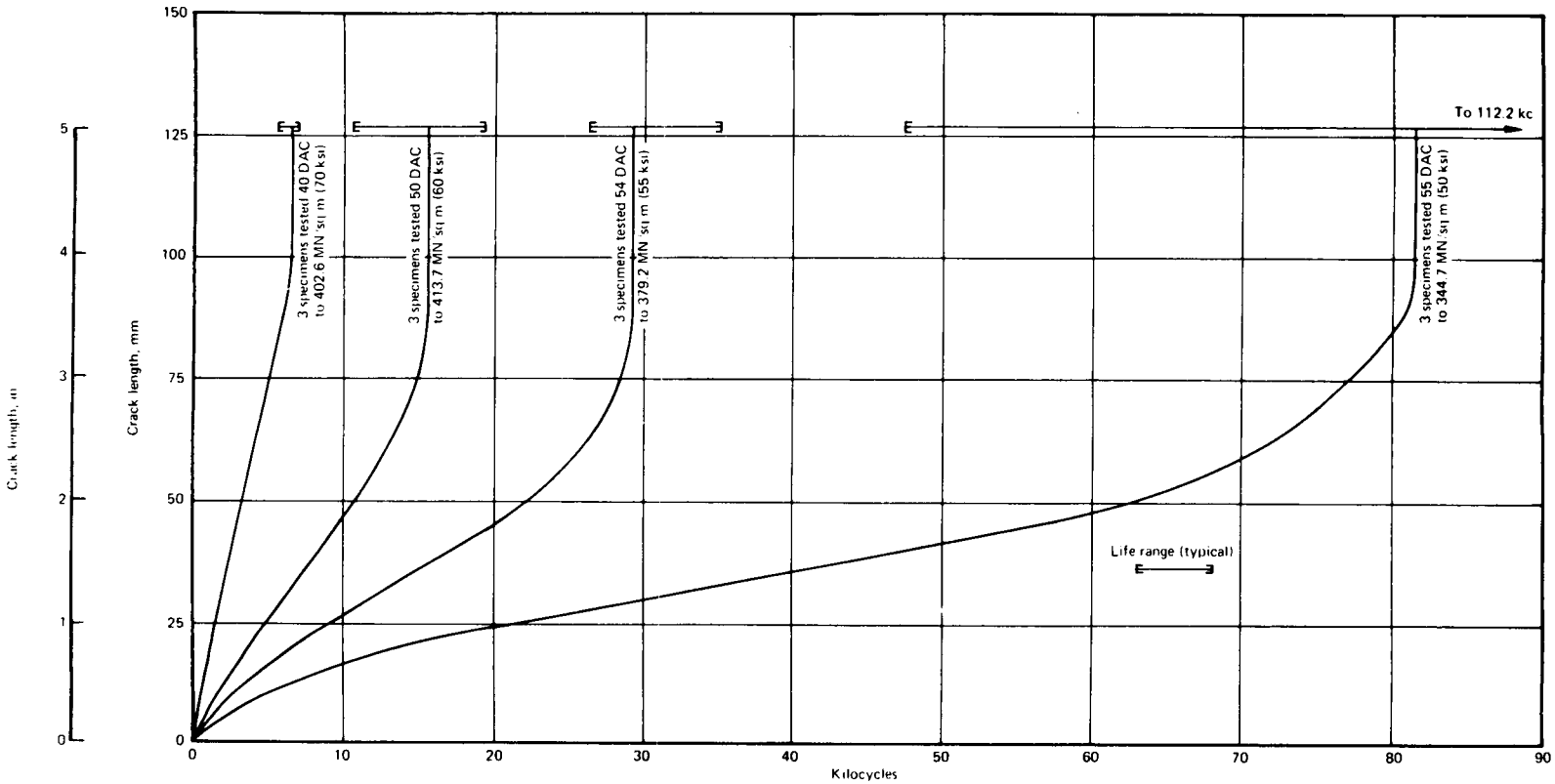

FIGURE 21.–CRACK LENGTH AS A FUNCTION OF CYCLES FOR CONFIGURATION 8

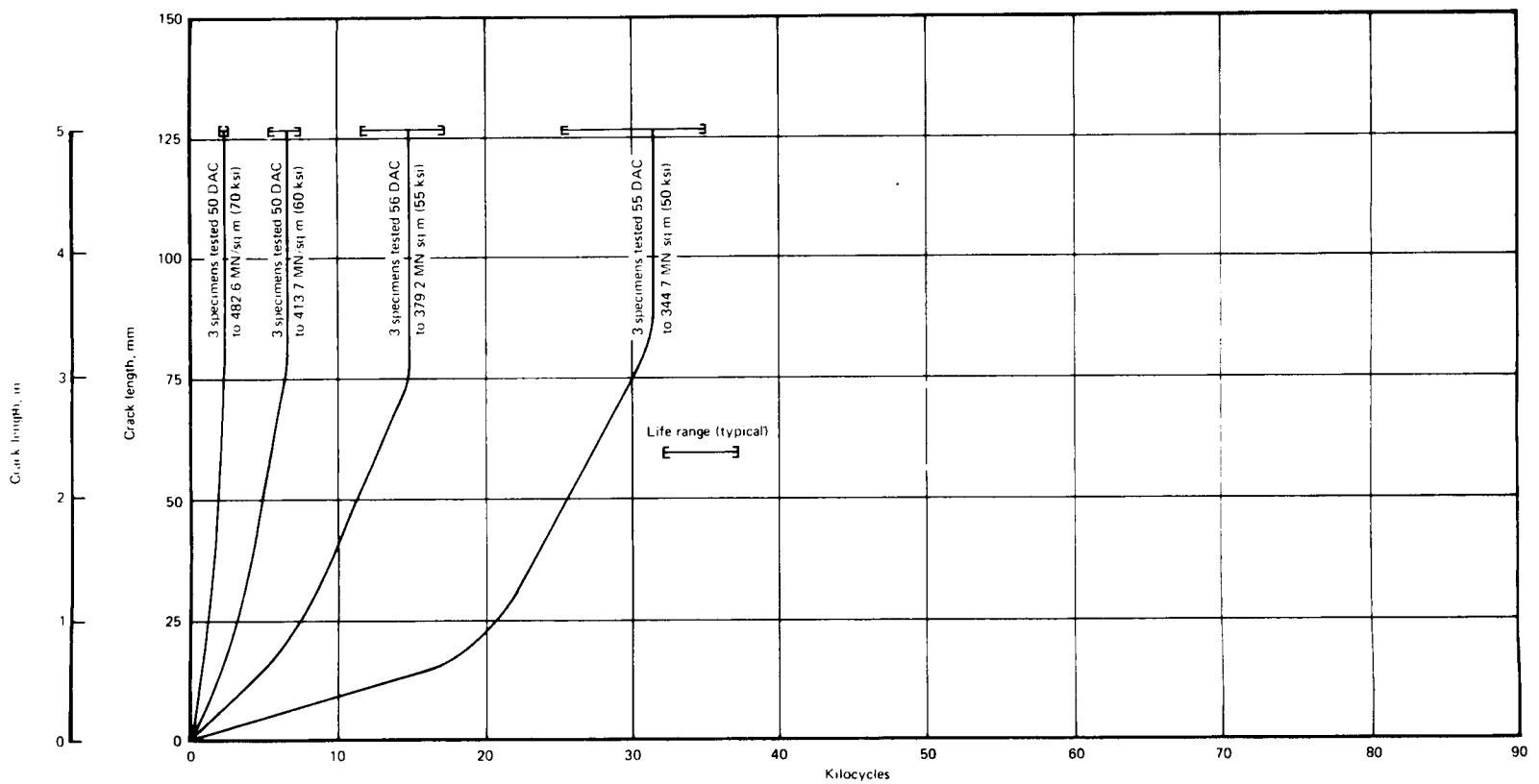

FIGURE 22.–CRACK LENGTH AS A FUNCTION OF CYCLES FOR CONFIGURATION 9

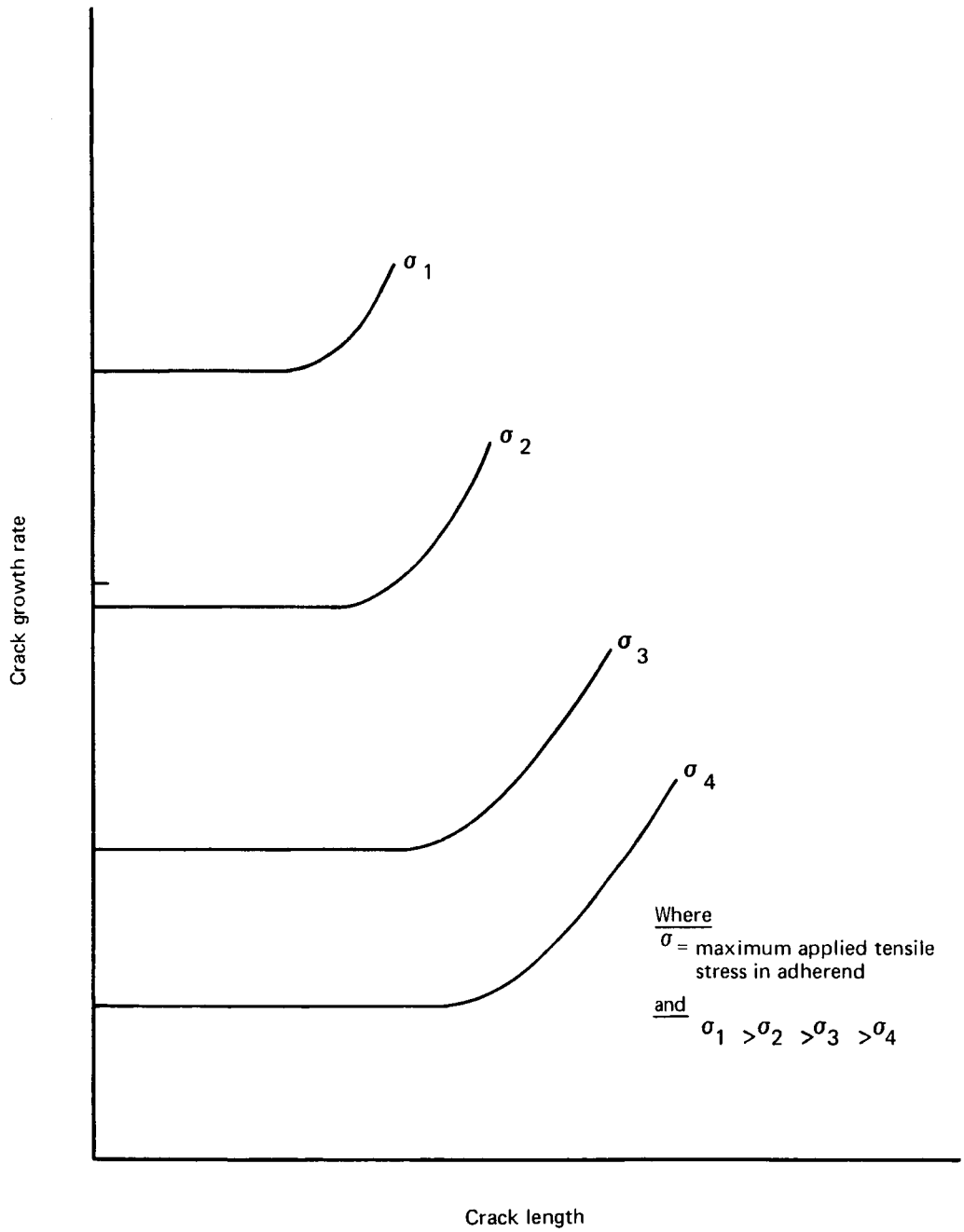

FIGURE 23.–ANTICIPATED CRACK GROWTH BEHAVIOR

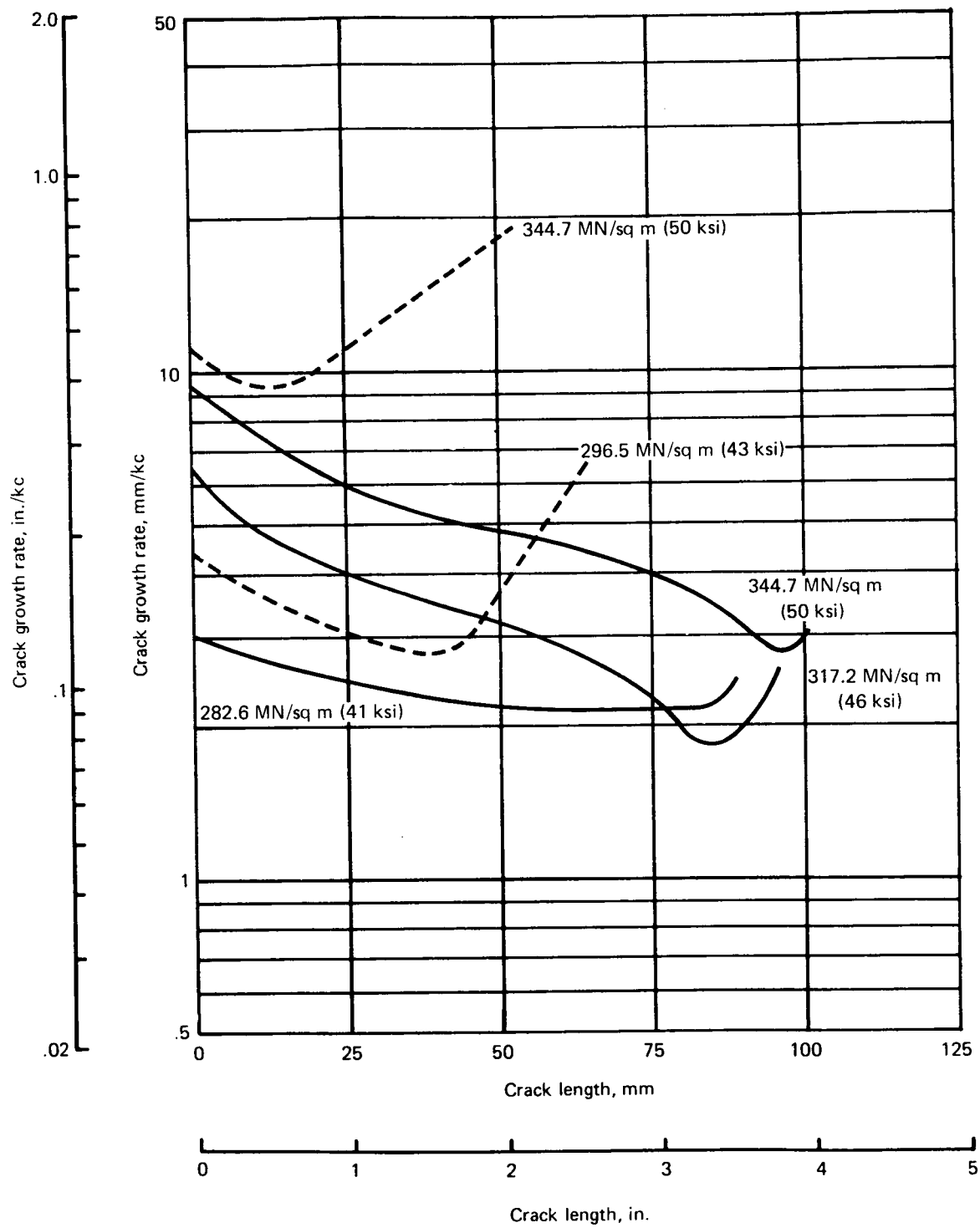

FIGURE 24.—CRACK GROWTH RATE AS A FUNCTION OF CRACK LENGTH FOR CONFIGURATION 1

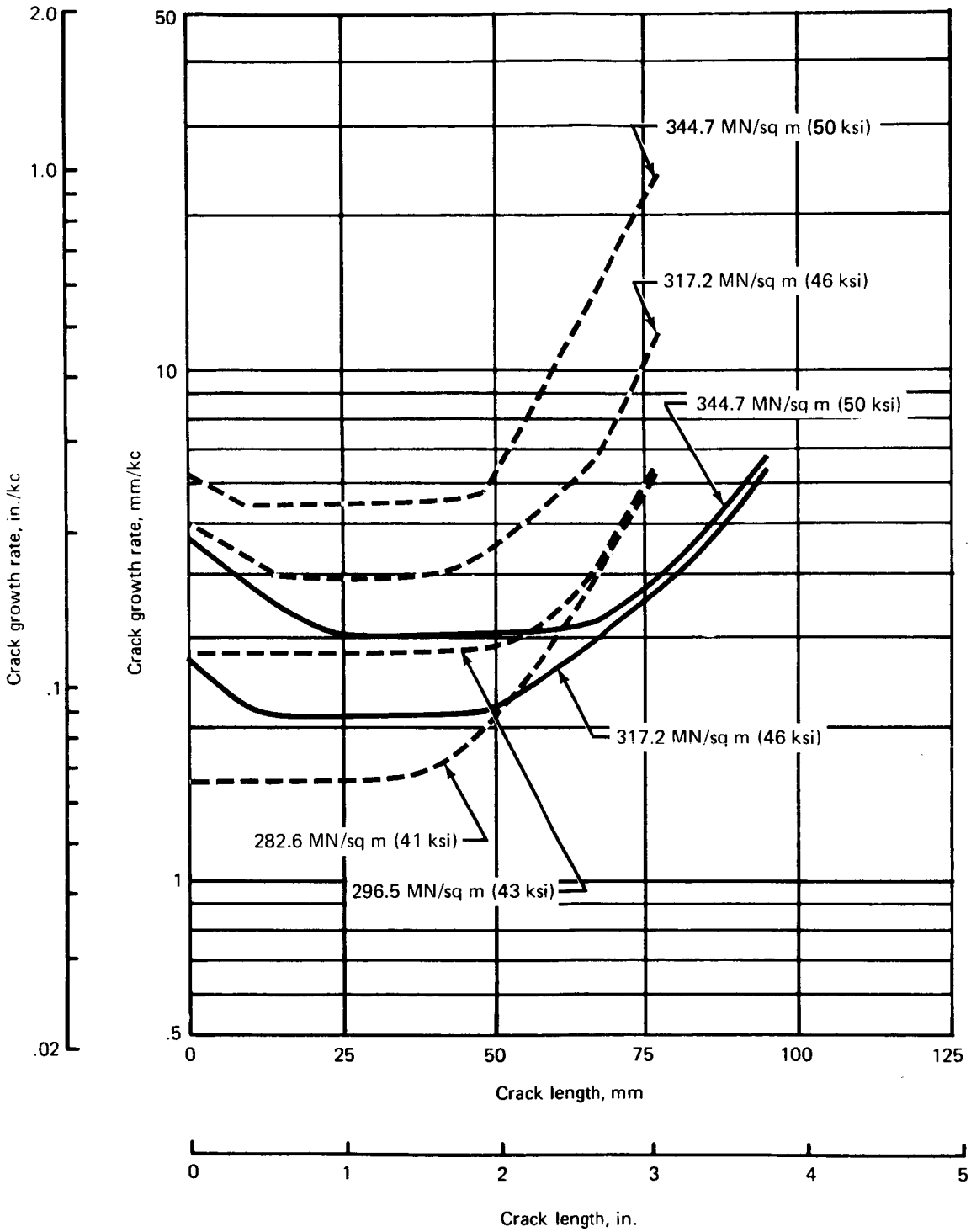

FIGURE 25.—CRACK GROWTH RATE AS A FUNCTION OF CRACK LENGTH FOR CONFIGURATION 2

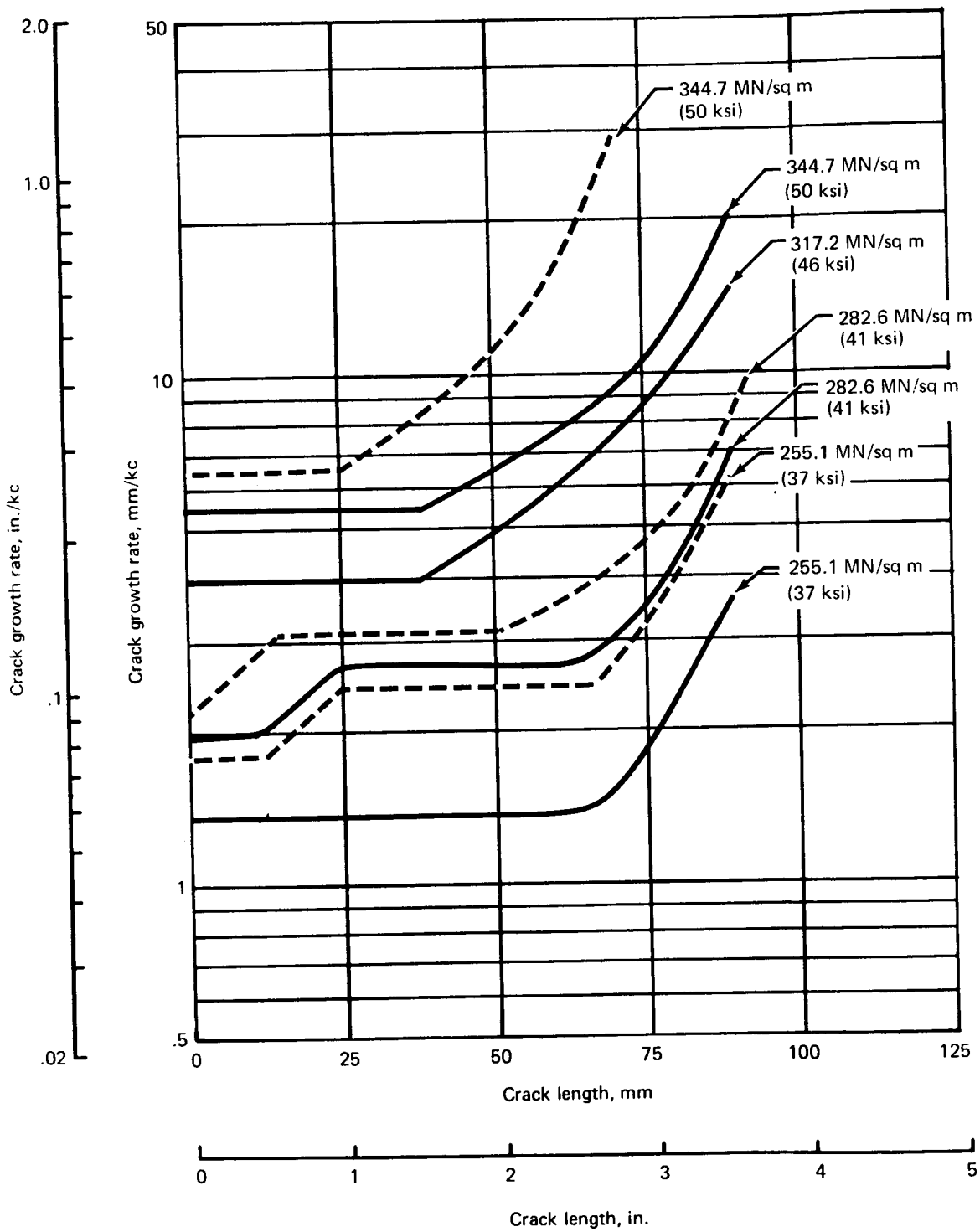

FIGURE 26.–CRACK GROWTH RATE AS A FUNCTION OF CRACK LENGTH FOR CONFIGURATION 3

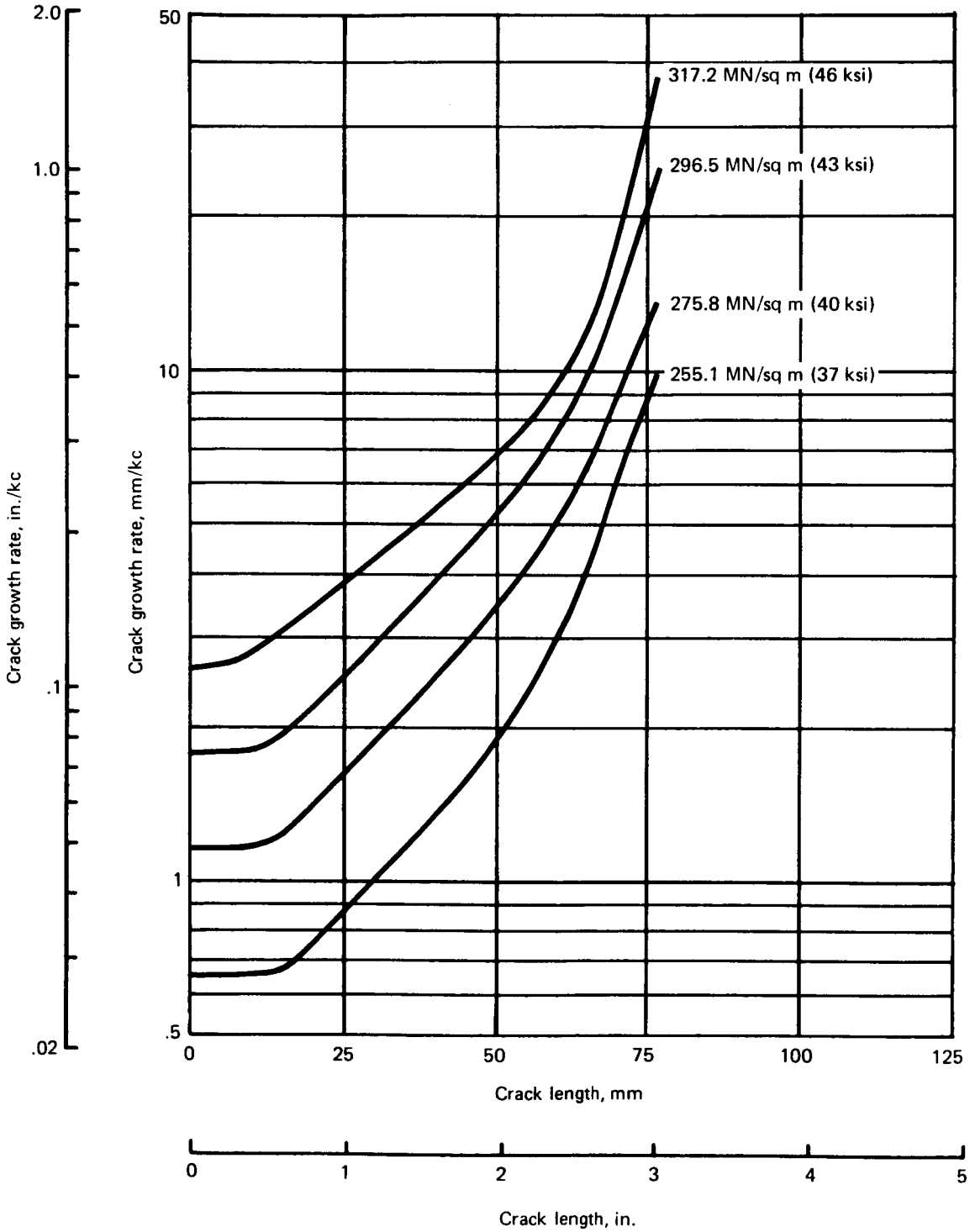

FIGURE 27.–CRACK GROWTH RATE AS A FUNCTION OF CRACK LENGTH FOR CONFIGURATION 4

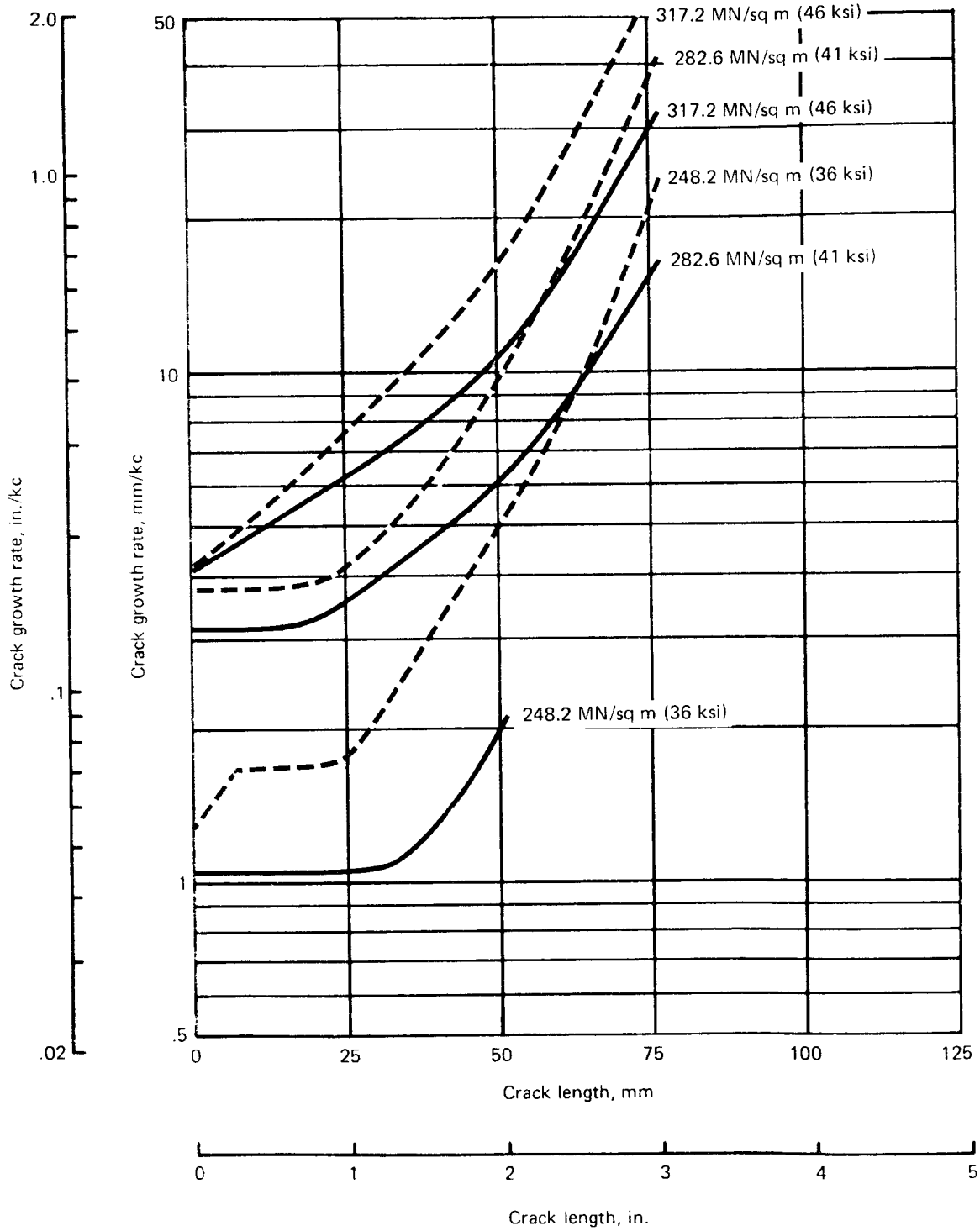

FIGURE 28.–CRACK GROWTH RATE AS A FUNCTION OF CRACK LENGTH FOR CONFIGURATION 5

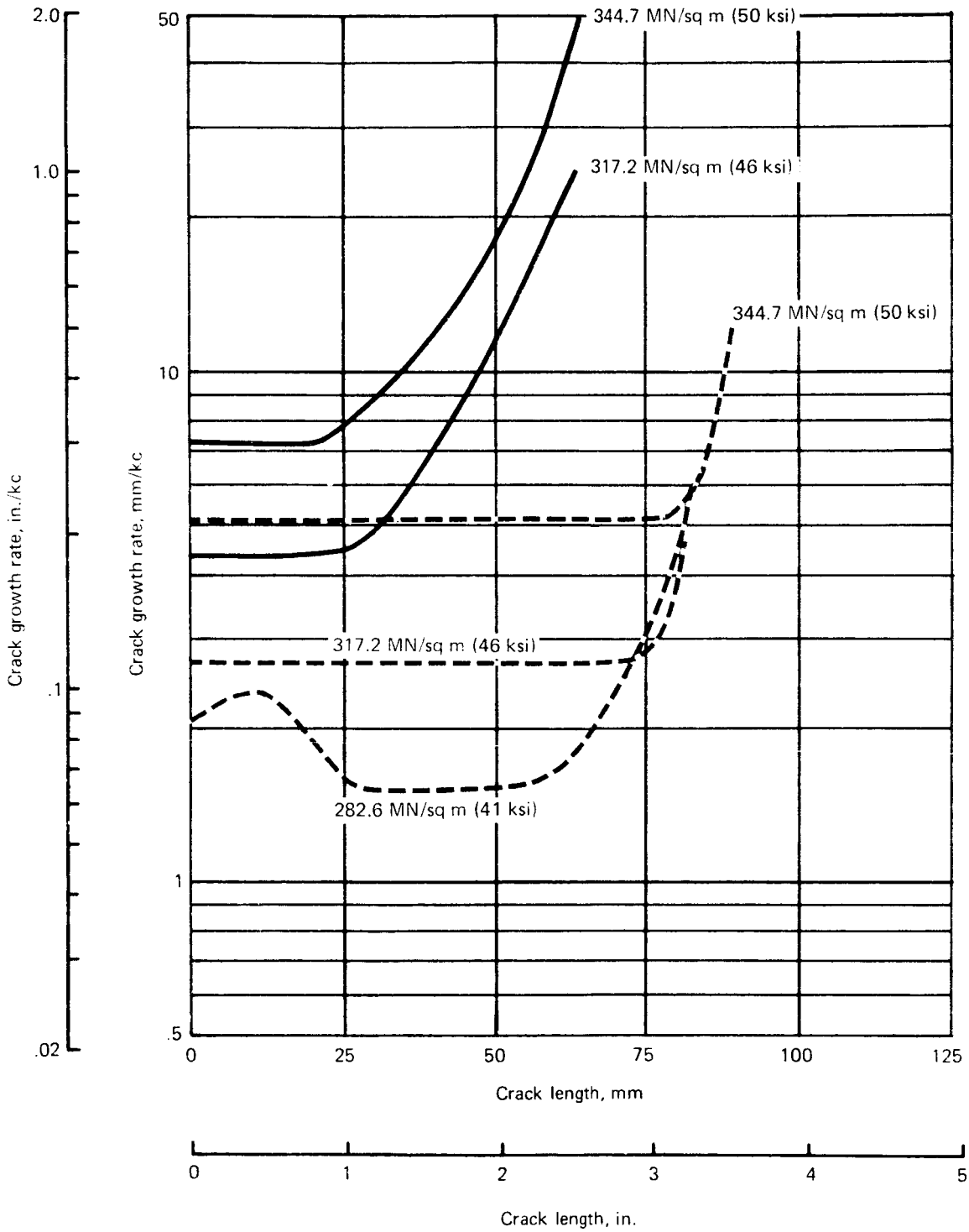

FIGURE 29.—CRACK GROWTH RATE AS A FUNCTION OF CRACK LENGTH FOR CONFIGURATION 6

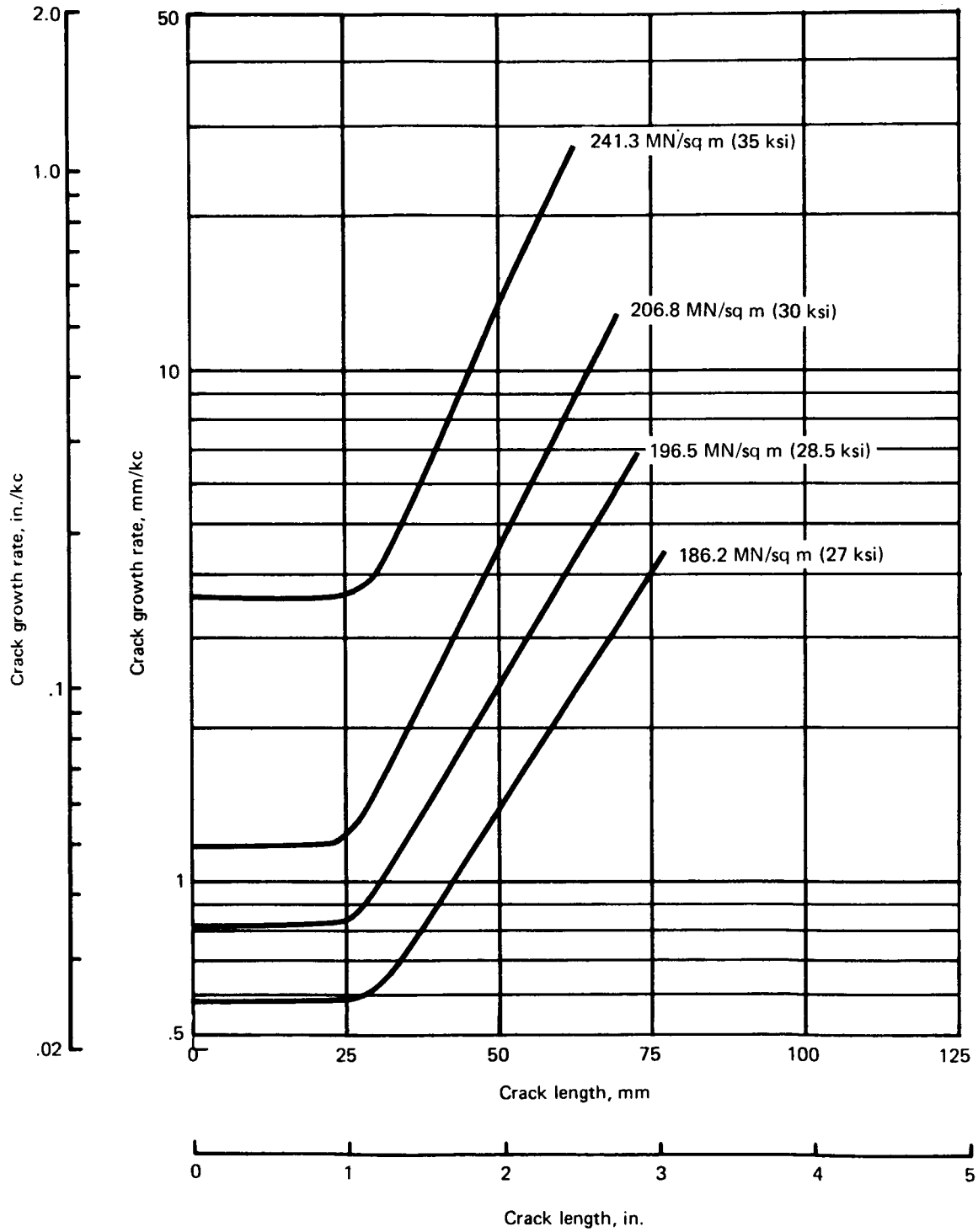

FIGURE 30.—CRACK GROWTH RATE AS A FUNCTION OF CRACK LENGTH FOR CONFIGURATION 7

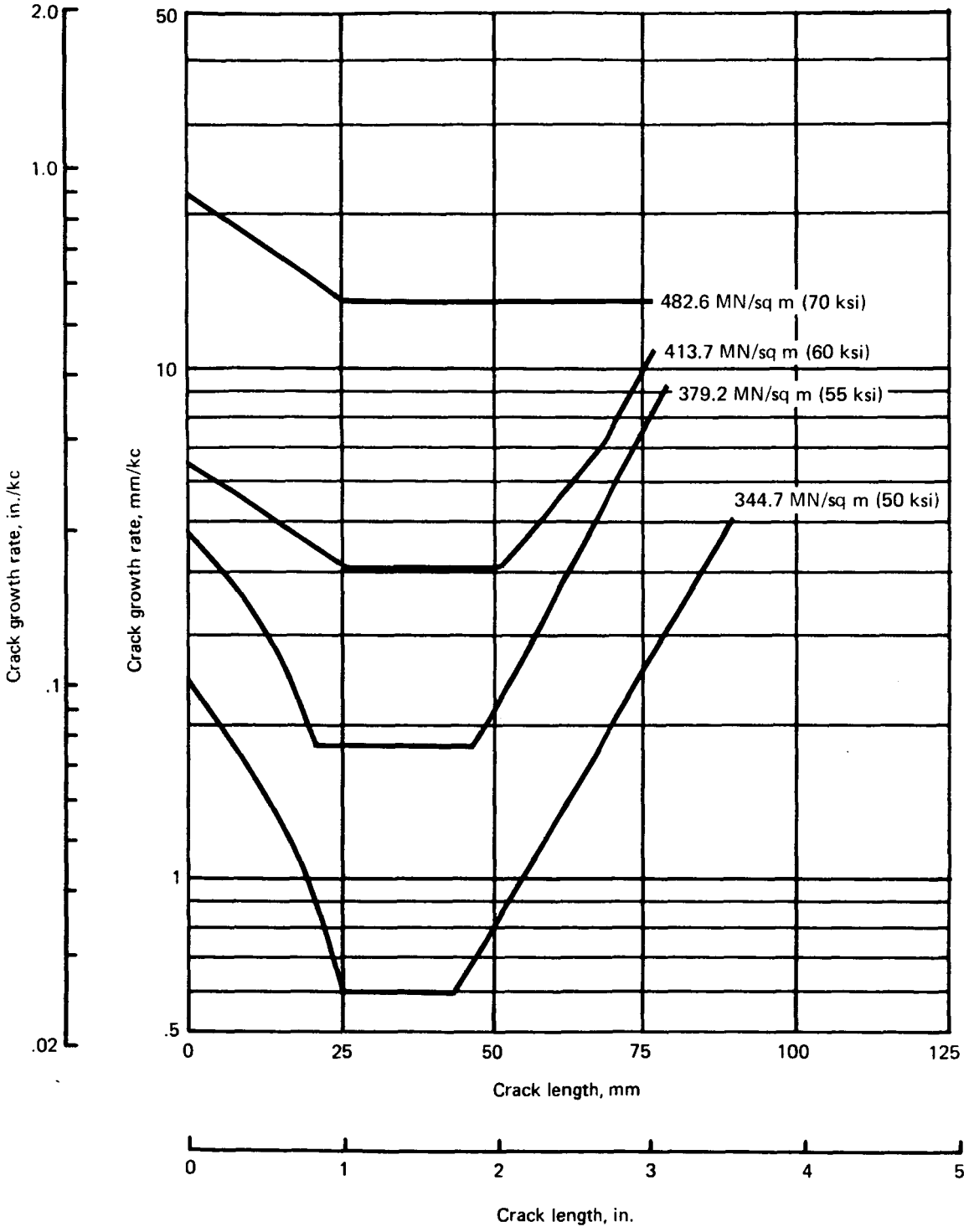

FIGURE 31.—CRACK GROWTH RATE AS A FUNCTION OF CRACK LENGTH FOR CONFIGURATION 8

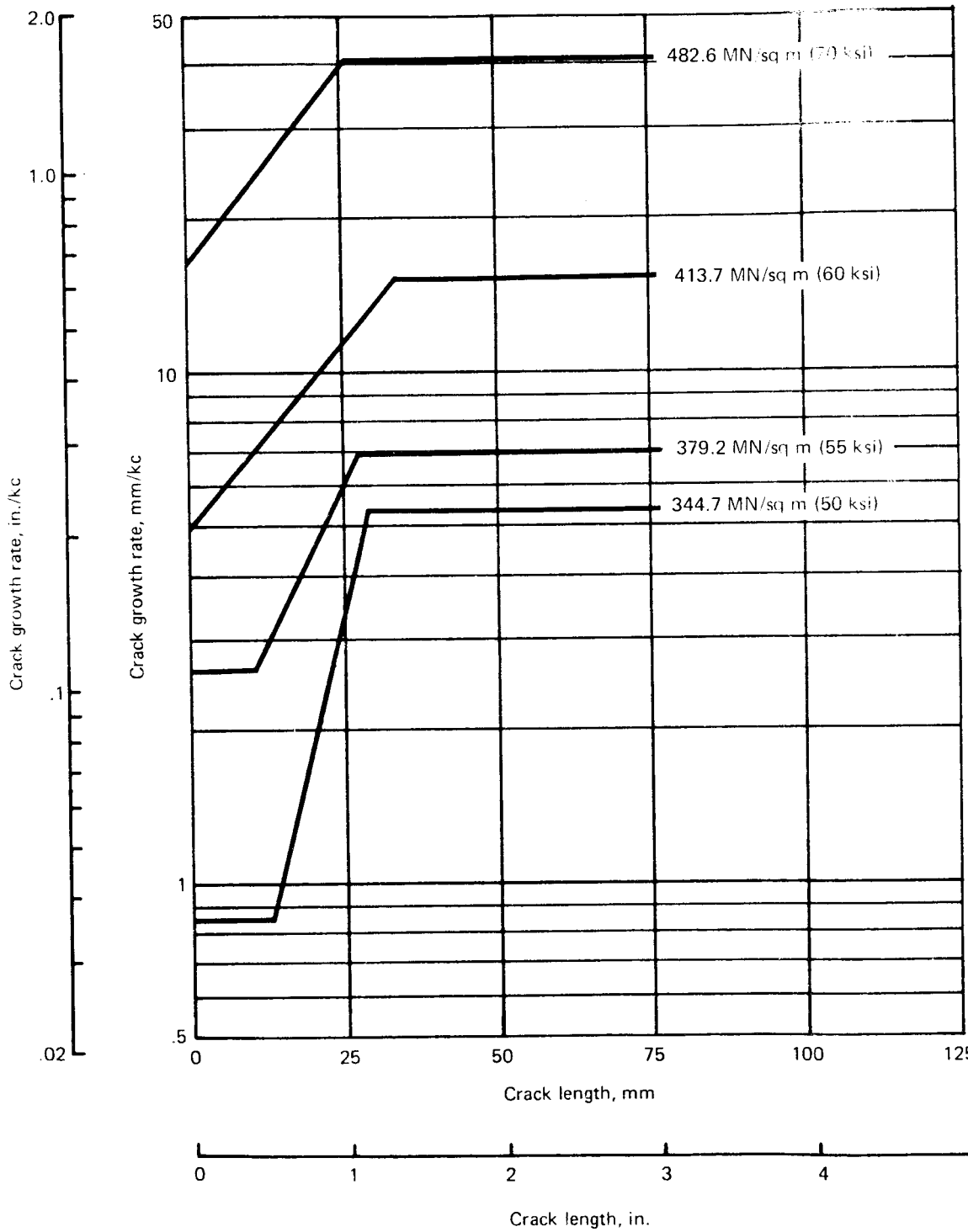

FIGURE 32.–CRACK GROWTH RATE AS A FUNCTION OF CRACK LENGTH FOR CONFIGURATION 9

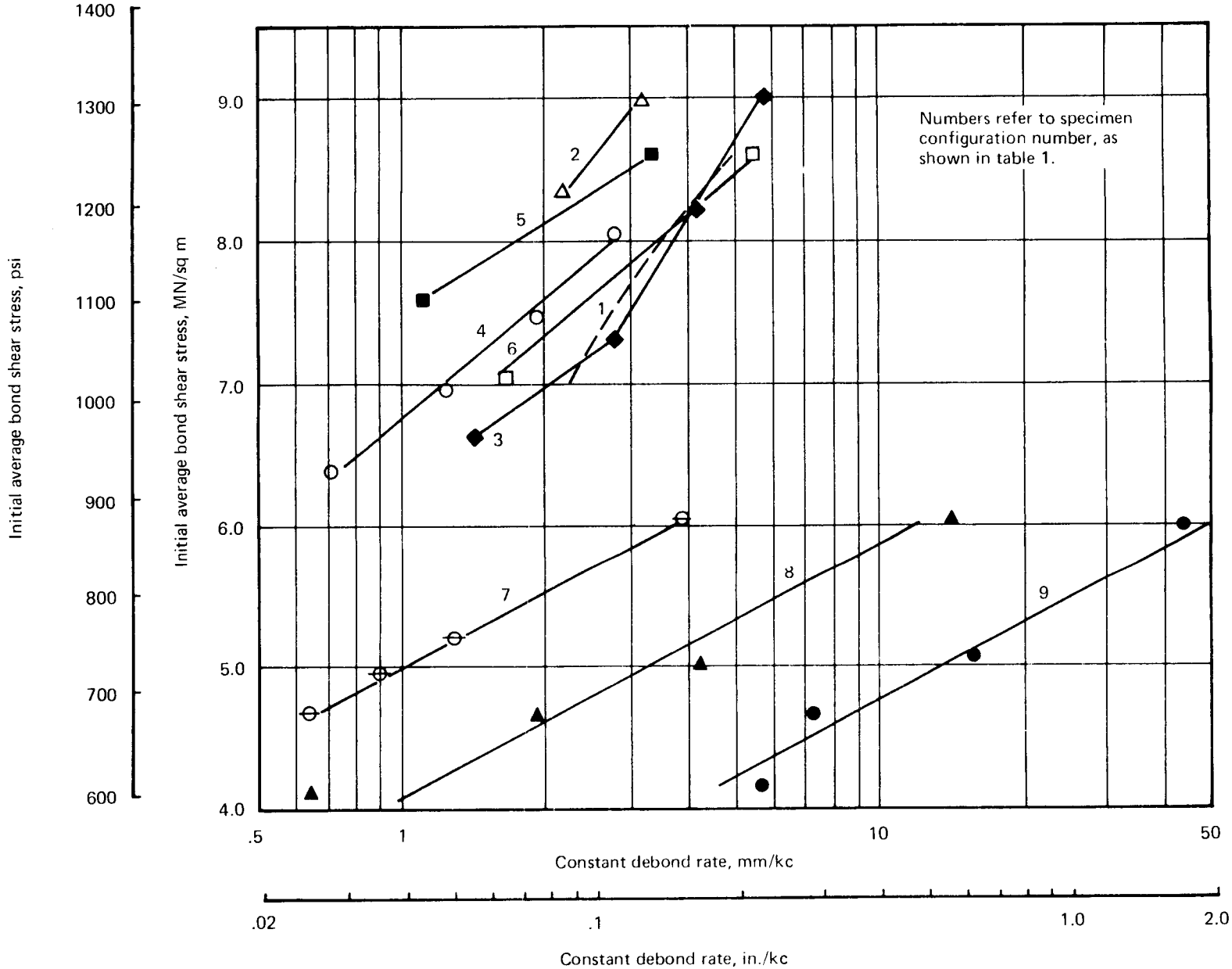

FIGURE 33.–CONSTANT DEBOND RATE AS A FUNCTION OF INITIAL AVERAGE BOND SHEAR STRESS

CONCLUSIONS

A study of the data obtained in this program provides the following general conclusions:

- Some specimens exhibited varying fatigue performance with different specimen ages. The general trend was toward reduced fatigue life with increased age; however, some specimens reversed this behavior.

- With the exception of the aging phenomenon, individual groups of specimens exhibited a low degree of scatter.

- Most specimens exhibited a constant debond rate early in the test. This was followed by a period of increasing debond rate and failure.

An examination of initial debond rate as a function of initial average bond shear stress provides the following conclusions regarding the effect of individual program variables:

- Specimens bonded with BP907 laminating resin debonded more rapidly than similar specimens bonded with AF-126 adhesive.

- The data suggest the existence of an optimum bondline thickness. Best performance was obtained with the medium thickness bondline. The thin bondline ranked next, while the thick bondline offered the least resistance to debonding early in the test.

- Reduced splice plate thickness to adherend thickness ratios resulted in reduced debond rates early in the test.

- Specimens bonded with a co-cure fabrication procedure resisted debonding better than specimens that were assembled with a sequential cure fabrication procedure.

- Test section width did not affect the early debond rate.

RECOMMENDATIONS

As a result of the data obtained in this program, the following recommendations are offered to further the understanding of the debonding phenomenon:

- A thorough study of the apparent aging effect should be made.
- Some specimens should be run with sufficient instrumentation to determine out-of-plane deformation.
- Additional advanced-composite specimens should be run to examine the effect of process method.

APPENDIX A

CONVERSION OF SI UNITS TO U.S. CUSTOMARY UNITS

The international system of units (SI) was adopted by the Eleventh General Conference on Weights and Measures, Paris, October 1960 (ref. 5). Conversion factors for the units used herein are given in table A-1. Prefixes to indicate multiples of units are given in table A-2.

TABLE A-1.–CONVERSION FACTORS FOR U.S. CUSTOMARY UNITS

Physical quantity	SI unit	Conversion factor*	U.S. customary unit
Length	Meter, m	39.3700	Inch, in.
Mass	Kilogram, kg	2.2046	Pound-mass, lbm
Load	Newton, N	0.2248	Pound-force, lbf
Density	Kilogram/meter^3, kg/m^3	0.000036	Pound-mass/inch^3, lbm/in.^{3}
		0.0624	Pound-mass/foot^3, lbm/ft^3
Load intensity	Newton/meter, N/m	0.0057	Pound-force/inch, lbf/in.
Modulus, stress, pressure	Newton/meter^2, N/m^2	0.000145	Pound-force/inch^2, psi
Temperature	Degree Kelvin, °K	$9/5(t_K)$-460	Degree Fahrenheit, °F

*Multiply the value in SI units by the conversion factor to obtain the value in U.S. customary units.

TABLE A-2.–PREFIXES FOR METRIC UNITS

milli, m	10^{-3}
kilo, k	10^3
mega, M	10^6
giga, G	10^9

APPENDIX B

TEST SPECIMEN MATERIALS

Aluminum sheet and plate were alloy 7075-T6 per QQ-A-250/13.

Titanium sheet was alloy 6Al-4V per MIL-T-9046F, type III, composition C, solution treated and aged.

Boron filaments were obtained from the Hamilton Standard Division of United Aircraft. These were 0.10 mm (0.004 in.) diameter filaments of boron vapor-deposited onto a tungsten wire substrate.

BP907 adhesive was obtained from the Bloomingdale Department of American Cyanamid Company. This is a film adhesive of epoxy resin impregnated into a scrim of type 104 glass fabric. The material thickness is 0.076 mm (0.003 in.). This is a latent cure material and has a shelf life of 6 months at room temperature. It is used primarily for drum winding with boron filament to form sheets of uncured boron-epoxy material. When used in adhesive bonding, liquid primer EC 2320 is used on all faying surfaces. The cure temperature cycle for the BP907 adhesive system is shown in figure B-1.

AF-126 adhesive was obtained from the Minnesota Mining and Manufacturing Company. This is a film adhesive of epoxy resin impregnated into a dacron fiber mat or veil. The material thickness is 0.13 mm (0.005 in.). Liquid primer EC 2320 is used on all faying surfaces. The cure temperature cycle for the AF-126 adhesive system is shown in figure B-2.

EC 2320 liquid primer was obtained from the Minnesota Mining and Manufacturing Company. This is a thermosetting, solvent base primer having 5% solids.

The test specimen material properties are listed in tables B-1 and B-2. Unless otherwise noted, values were obtained from MIL-HDBK-5 (ref. 7).

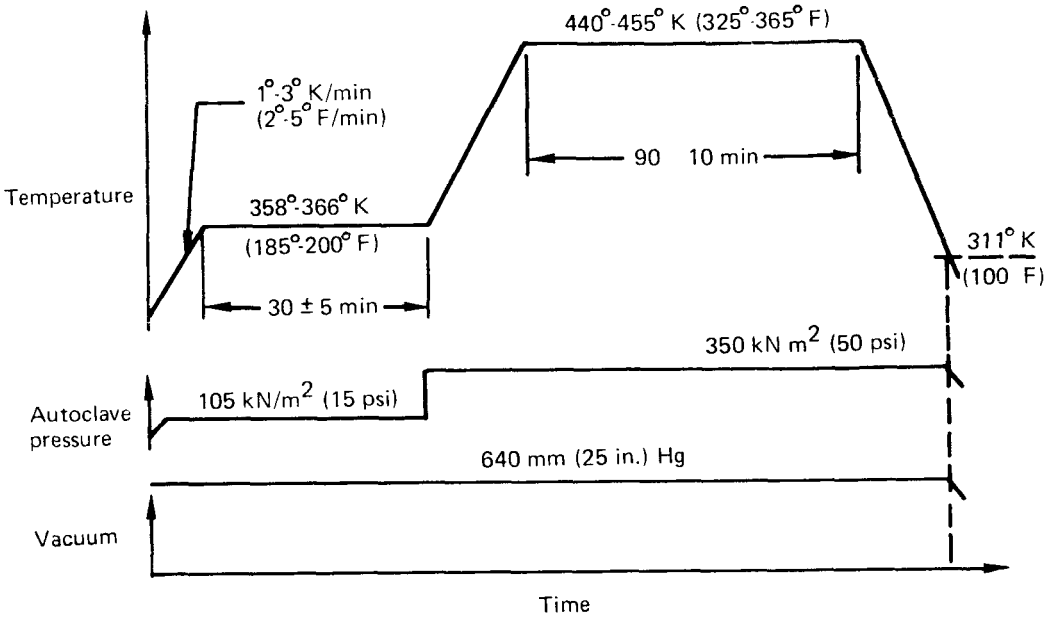

FIGURE B-1.–CURE CYCLE FOR BP907 ADHESIVE SYSTEM

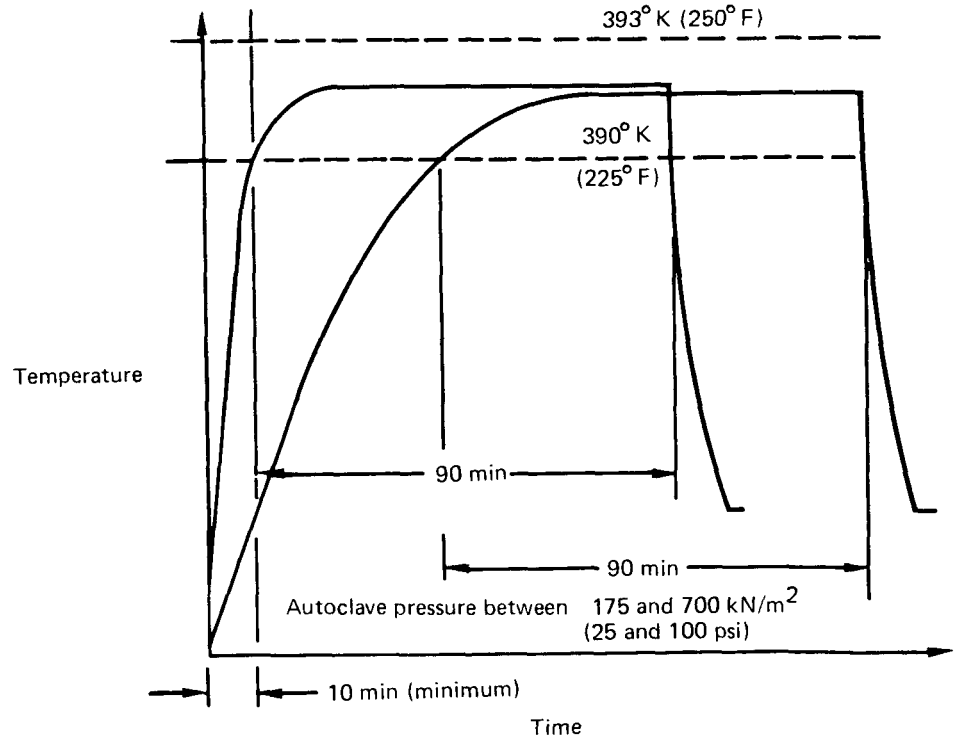

FIGURE B-2.–CURE CYCLE FOR AF-126 ADHESIVE SYSTEM

TABLE B-1.—ROOM TEMPERATURE PROPERTIES OF METALS

Property	Ti-6Al-4V heat treated and aged	7075-T6 aluminum
Tensile ultimate, MN/m^2 (ksi)	1081 (157)	523 (76)
Tensile yield, MN/m^2 (ksi)	985 (143)	447 (65)
Compressive yield, MN/m^2 (ksi)	1047 (152)	461 (67)
Shear ultimate, MN/m^2 (ksi)	675 (98)	317 (46)
Elongation % in 51 mm (2.0 in.)	3	7
Modulus of elasticity, $N/m^2 \times 10^9$ (psi x 10^6)	110.2 (16.0)	70.9 (10.3)
Compressive modulus, $N/m^2 \times 10^9$ (psi x 10^6)	113.0 (16.4)	72.3 (10.5)
Shear modulus, $N/m^2 \times 10^9$ (psi x 10^6)	42.7 (6.2)	26.8 (3.9)
Poisson's ratio	0.30	0.33
Coefficient of thermal expansion, mm/mm x 10^6 per °K (in./in. x 10^6 per °F)	9.9 (5.3)	23.2 (12.9)

TABLE B-2.—ROOM TEMPERATURE PROPERTIES OF BORON, RESIN, AND UNIDIRECTIONAL BORON-RESIN COMPOSITE

Property	Material		
	BP907*	Boron filament	Boron/BP907
Boron volume/composite volume	–	–	0.485
Tensile modulus longitudinal, $N/m^2 \times 10^9$ (psi $\times 10^6$)	8.1 (1.17)	413 (60)	201 (29.1)
Tensile modulus transverse, $N/m^2 \times 10^9$ (psi $\times 10^6$)	8.1 (1.17)	–	16.1 (2.34)
Compressive modulus longitudinal, $N/m^2 \times 10^9$ (psi $\times 10^6$)	8.1 (1.17)	413 (60)	201 (29.1)
Compressive modulus transverse, $N/m^2 \times 10^9$ (psi $\times 10^6$)	8.1 (1.17)	–	16.1 (2.34)
Shear modulus, $N/m^2 \times 10^9$ (psi $\times 10^6$)	3.11 (0.452)	172 (25)	8.38 (1.22)
Poisson's ratio	0.30	0.20	0.246
Coefficient of thermal expansion, mm/mm $\times 10^6$ per °K (in./in. $\times 10^6$ per °F)	28.0 (15.0)	4.9 (2.7)	5.8 (3.1)

*Includes scrim.

APPENDIX C

TEST SPECIMEN FABRICATION PROCEDURES

Surface Preparation

Proper surface preparation was essential to attaining a good adhesive bond. The surface preparation operations were controlled by Boeing process documents. The process for each material is summarized briefly as follows:

- Aluminum–Vapor degrease, alkaline clean, deoxidize, protective wrap, prime within 16 hours.
- Titanium–Solvent clean, alkaline clean, deoxidize, phosphate fluoride conversion coat, protective wrap, prime within 16 hours.
- Boron-epoxy–No surface preparation required. Surface protected by nylon peel ply and aluminum protective tape.

Boron-Epoxy Splice Plate Fabrication

All boron-adhesive tape material was fabricated by a drum-winding process. Tapes 0.254 m (10 in.) wide by 1.83 m (72 in.) long were wound, four at a time, on a cylindrical mandrel. All boron-epoxy tapes were wound on BP907 adhesive film. Tapes were wound at 8.2 filaments per millimeter (208 filaments per inch) of width with a filament tension of 0.67 to 0.98 N (0.15 to 0.22 lb) pull. After winding, tapes were cut across the width removed from the mandrel, individually packaged in plastic film, and marked with identification numbers. Tapes were then stored at 255.38°K (0°F) until required for layup in a bond assembly.

Composite splice plates were laminated as follows. A flat tool plate was provided. Tapes were cut to the 38.1 mm (1.5 in.) width. Initially a layer of nylon peel ply was laid on the tool with the adhesive side up. Successive layers of boron composite were then laid, adhesive side down, until the required number of plies was achieved. A picture frame was placed around the periphery of the laminate to maintain dimensional tolerance. The plate with laminated plies was then vacuum bagged and cured to form long lengths of boron-epoxy splice plate stock.

Following cure, the long lengths of splice plate stock were further protected by a layer of aluminum tape placed over the nylon peel ply. This stock was then bandsawed into approximately 150 mm (6.0 in.) lengths. A final operation dressed the ends of the splice plates with a grinding wheel.

Structural Adhesive Bonding

The bonding processes employed for the fabrication of cyclic debonding specimens were controlled by Boeing process documents. Bonding was accomplished in production shops using positive-pressure, air-heated autoclaves. Cure cycles for the BP907 and AF-126 adhesive systems are shown in figures B-1 and B-2. Lap shear and peel process control panels were processed with each bond cycle involving aluminum specimens. Following cure, specimens were checked for voids and porosity using through-transmission ultrasonics.

REFERENCES

1. Hoffman, D. J. and June, R. R.: Cyclic Debonding of Adhesive Joints: Data Report. D6-60136-5, Boeing Commercial Airplane Company, 1973. (Available as NASA CR-112219, 1973.)

2. Oken, S. and June, R. R.: Analytical and Experimental Investigation of Aircraft Metal Structures Reinforced with Filamentary Composites, Phase I, Concept Development and Feasibility. D6-60136, The Boeing Company, 1970. (Available as NASA CR-1859, 1971.)

3. Blichfeldt, B. and McCarty, J. E.: Analytical and Experimental Investigation of Aircraft Metal Structures Reinforced with Filamentary Composites, Phase II, Structural Fatigue, Thermal Cycling, Creep, and Residual Strength. D6-60136-2, The Boeing Company, 1971. (Available as NASA CR-2039, 1972.)

4. Bryson, L. L. and McCarty, J. E.: Analytical and Experimental Investigation of Aircraft Metal Structures Reinforced with Filamentary Composites, Phase III, Major Component Development. D6-60136-3, The Boeing Company. (Available as NASA CR-2122, 1973.)

5. Comm. on Metric Pract.: ASTM Metric Practice Guide. NGS Handbook 102, U.S. Department of Commerce, March 10, 1967.

6. Baud, R. V.: Product Eng. V5, 1934, p. 133.

7. Anon.: Metallic Materials and Elements for Aerospace Vehicle Structure. Military Handbook MIL-HDBK-5, U.S. Department of Defense.

☆ U. S. GOVERNMENT PRINTING OFFICE: 1973—736-650/18 REGION NO. 3-11.